

11

Structure, Mechanics, and Rheology of Concentrated Emulsions and Fluid Foams

H. M. Princen

Consultant, Flemington, New Jersey, U.S.A.

I. BACKGROUND

Whether enjoying the luxury of a bubble bath or enduring the drudgery of washing dishes, one is likely to be struck by the beauty and intricate structure of foams, froths, or “suds.” Keen observers may even notice the unusual elastic and yield properties, not seen in the constituent aqueous and gaseous phases. Scientifically, the interest in and the study of foams have been truly multidisciplinary and have not been confined to chemists, engineers, and physicists. Foams have traditionally inspired mathematicians for their geometric properties and as equilibrium structures in which the surface area is minimized (1). Metallurgists (2) have realized the similarity between foams and polycrystalline metals, both in their structure and coarsening behavior (grain growth). Similarly, botanists and life scientists in general have noticed strong structural parallels between foams and living tissues (3).

Gas–liquid foams are abundant in nature and their technological applications are numerous. They are used to advantage in fire fighting, enhanced oil recovery, foods (e.g., whipped cream), cosmetics (e.g., shaving cream), and in many other ways. The “world of foams” may be considerably expanded by the realization that concentrated liquid–liquid emulsions, although generally characterized by a much smaller mean size of the dispersed units, are structurally identical to gas–liquid foams, which is readily revealed under the microscope. Macroscopically, they behave like

viscoelastic gels, mayonnaise being a good example. Such emulsions have been variously referred to as high-internal-phase-ratio emulsions (HIPREs), biliquid foams, “aphrons,” or, simply, highly concentrated emulsions. Although they lack the compressibility of gas–liquid foams, they behave similarly in all other respects. Detailed study of such emulsion systems started rather recently and may perhaps be traced to the attempts of Lissant (4–6) and Beerbower et al. (7–10) to design safer aviation and rocket fuels, in which fuel droplets are tightly packed inside a continuous aqueous phase. Reverse (i.e., concentrated water-in-oil) systems can be readily prepared as well. They find application in the high-explosives area, but have particular appeal in the foods and cosmetics industries. What entrepreneur’s mouth would not water at the prospect of being able to sell a product that is at least 90% water and yet is luxuriously rich and creamy? Lissant, in particular, patented numerous potential applications in these areas (e.g., Ref. 11). In yet other applications, the oil phase, either external or internal, can consist of a polymerizable monomer. Subsequent polymerization by heat or radiation can lead to interesting polymers or structurally unique materials (e.g., Refs. 6 and 12–16).

Because of all of these scientific and technological aspects, a thorough understanding of foams and concentrated emulsions is highly desirable. In response to this need, there has lately been a clear upsurge in interest, again from a variety of disciplines, and considerable progress has been and is being made. Several comprehensive textbooks on emulsions and foams have recently been published (17–22). We believe that the overlap with this review is minimal.

II. INTRODUCTION

In general, when a fluid phase (liquid or gas) is dispersed in an immiscible liquid to form drops or bubbles, there is a tendency for the phases to separate again to reduce the augmented surface free energy. With pure phases, this proceeds by rapid coalescence of approaching dispersed entities, as there is no barrier against rupture of the intervening liquid film. Stability or, more correctly, metastability can be conferred by adsorption of surfactants, polymers, or finely divided solid particles at the interface. By this expedient, coalescence can often be suppressed completely. However, this will not prevent ultimate phase separation, as there is another mechanism for reducing the surface area, namely Ostwald ripening. By this mechanism, large bubbles or drops grow at the expense of small ones by dissolution and diffusion of the dispersed phase in response to the higher Laplace pressure in the latter ones. Because gases tend to have greater solubility and diffusivity

in a given continuous liquid than do most other liquids, this process is generally much more rapid in foams than in emulsions. Indeed, whereas most foams will not survive for more than a few hours—even in the absence of coalescence—it is relatively easy to prepare concentrated emulsions whose drop size distribution does not change perceptibly for months or years. They are kinetically or operationally (although not thermodynamically) stable. For this and many other reasons, emulsions may be better characterized and their properties more reliably investigated experimentally than is possible with foams. Thus, to learn about *foam* behavior through experiments, we recommend one look at concentrated emulsions instead. In the same vein, we may use the terms “bubble” and “drop” interchangeably.

In this review, we will only consider stable dispersions, in which coalescence has been totally suppressed. We further restrict ourselves to highly concentrated dispersions, in which the volume fraction of the dispersed phase, ϕ , exceeds a critical value ϕ_0 where the properties start to change drastically. This critical volume fraction corresponds to that of a system of close-packed spheres having the same drop volume distribution as the dispersion. The term “close packed” is somewhat ambiguous and the corresponding volume fraction is not always clearly defined and/or established. Although monodisperse spheres can, in principle, be packed to a maximum density of $\phi_0 = 0.7405$, this value is rarely achieved. In practice, one is more likely to achieve only *random* close packing, which is considerably less dense ($\phi_0 \approx 0.64$) due to the voids created by “arching.” There is a persistent myth that the packing density of a *polydisperse* system is characterized by $\phi_0 > 0.7405$. It is true that the voids in a close-packed system of spheres can be filled sequentially with smaller and smaller spheres of very specific sizes until $\phi_0 \approx 1$. However, this would require a unique multimodal size distribution as well as a unique spatial distribution, neither of which are likely to be ever encountered in practice. It is our experience with typical, unimodal polydisperse emulsions that the spherical droplets arrange themselves at a packing density that, although considerably larger than the 0.64 expected for the random close-packed monodisperse case, is close to but slightly *smaller* than 0.74. Although the actual value must depend somewhat on the details of the size distribution, we estimate that $0.70 < \phi_0 < 0.74$ in most practical cases, where conventional means are used to prepare the emulsion (23,24).

There are reasons why the *effective* value of ϕ , including that of ϕ_0 , may deviate from the apparent value. If the thickness, h , of the stabilized film of continuous phase, separating the dispersed drops or bubbles, is not insignificant compared to the drop or bubble radius, R , then the effective volume of each drop must be augmented by that of a surrounding sheath of thickness $h/2$. This leads to a somewhat larger effective volume fraction,

ϕ_e , which is given (23) by

$$\phi_e = \phi \left[1 - \left(\frac{\phi}{\phi_0} \right)^{1/3} \frac{h}{2R} \right]^{-3} \approx \phi \left(1 + \frac{3.15h}{2R} \right) \quad (1)$$

The latter form is a good approximation for any $\phi > \phi_0$ and $h/R \ll 1$. In most foams, the effect is expected to be minimal, as the bubbles tend to be relatively large. For emulsions of small drop size, however, the effect may be considerable and the peculiar properties resulting from extreme crowding may commence at an apparent volume fraction that is considerably smaller than one would expect for zero film thickness. For example, in an emulsion with droplets of $2R = 1 \mu\text{m}$ and $h = 50 \text{ nm}$, the effective volume fraction already reaches a value of 0.74 at an apparent volume fraction of only about 0.64! The finite film thickness may, for example, result from electrostatic double-layer forces (25) or adsorbed polymers. In what follows, we shall assume zero film thickness, with the understanding that Eq. (1) is to be invoked whenever $h/R \neq 0$.

Another complication arises when strong attractive forces operate between the drops or bubbles. This may lead to a finite contact angle, θ , between the intervening film (of reduced tension) and the adjacent bulk interfaces (23,26–28). Under those conditions, droplets will spontaneously deform into truncated spheres upon contact and can thus pack to much higher densities. For monodisperse drops, the ideal close-packed density, consistent with minimization of the system's surface free energy, is given (23) by

$$\phi_0(\theta) = 0.7405 \left(-\frac{5}{\cos^3 \theta} + \frac{9}{\cos^2 \theta} - 3 \right) \quad (2)$$

which is valid up to $\theta = 30^\circ$, where $\phi_0 = 0.964$. For $\theta = 0$, we recover $\phi_0 = 0.7405$, and ϕ_0 is expected to reach unity when θ exceeds 35.26° (23,28). In the latter limit, all of the continuous phase (except that in the intervening films) should, in principle, be squeezed out spontaneously. In practice, however, one tends to find just the opposite; that is, when θ is large, the droplets spontaneously flocculate into a rather open structure in which $\phi_0 < 0.7405$. The situation is similar to that of a flocculated solid dispersion whose sediment volume is generally greater than that of a stable dispersion. Apparently, the strong attractive forces prevent the droplets from sliding into their energetically most favorable positions, leaving large voids in the otherwise dense structure. Nevertheless, the structure may be irreversibly densified to approach the condition prescribed by Eq. (2) by centrifugation and subsequent relaxation (23,27). Foams and emulsions in which $\theta \neq 0$ have only been studied occasionally and will rarely be touched upon in this review.

III. STRUCTURAL ELEMENTS

As discussed earlier, the nature and properties of fluid–fluid dispersions start to change drastically when the volume fraction approaches or exceeds ϕ_0 . A certain rigidity sets in, because the drops or bubbles can no longer move freely past each other.

As the volume fraction is raised beyond ϕ_0 , the drops lose their sphericity and are increasingly deformed while remaining separated by thin stable films of continuous phase. At sufficiently high ϕ , the drops become distinctly polyhedral, albeit with rounded edges and corners. At this stage, the continuous phase is confined to two structural elements: *linear* Plateau borders with an essentially constant cross section over some finite length, and *tetrahedral* Plateau borders, where four linear borders converge (Fig. 1a).

Each linear border is generally curvilinear and fills the gap between the rounded edges of three adjoining polyhedral drops. In cross section, its sides are formed by three arcs, each pair of which meets tangentially to form the thin film separating the corresponding droplet pair (Fig. 1b). The pressures in the drops are related to the mean curvatures of the intervening films through

$$\begin{aligned} p_1 - p_2 &= 2\sigma C_{12} \\ p_2 - p_3 &= 2\sigma C_{23} \\ p_3 - p_1 &= 2\sigma C_{31} \end{aligned} \quad (3)$$

where σ is the interfacial tension between the continuous and dispersed phases and the sign of each film curvature C is taken positive (negative)

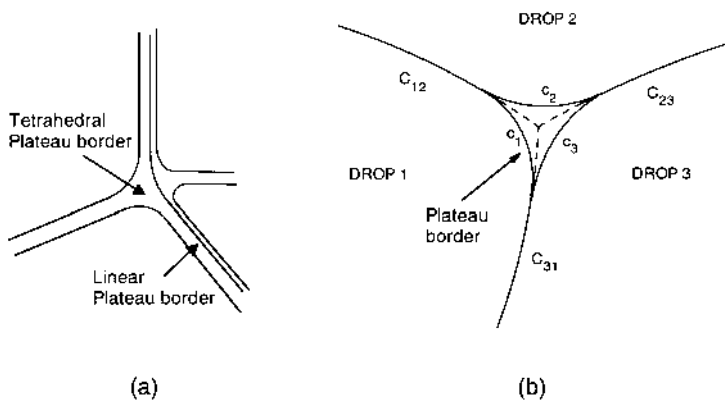


Figure 1 (a) Four linear Plateau borders meeting in a tetrahedral plateau border; (b) cross section through a linear Plateau border and its three associated films and drops.

if the pressure in the drop indicated by the first index is the higher (lower) one. Adding Eqs. (3) leads to the following relationship between the three mean film curvatures:

$$C_{12} + C_{23} + C_{31} = 0 \quad (4)$$

The pressure inside the linear Plateau border, p_b , is given by

$$p_b = p_1 - \sigma c_1 = p_2 - \sigma c_2 = p_3 - \sigma c_3 \quad (5)$$

where c_1 , c_2 , and c_3 are the curvatures of the border walls and are all counted as positive. Since all Plateau borders are connected, they are in hydrostatic equilibrium.

Normally, an ambient gaseous atmosphere of pressure P surrounds the dispersion. Relative to this ambient pressure, p_b is lower and given (29) by

$$p_b = P - \sigma_c |C_t| \quad (6)$$

where $|C_t|$ is the absolute value of the curvature of the free continuous-phase surface at the dispersion–atmosphere boundary (i.e., *between* the exposed bubbles) and σ_c is the *surface tension* of the continuous phase [$\sigma_c = \sigma$ for foams, but $\sigma_c \neq \sigma$ for emulsions (29) unless the “ambient atmosphere” consists of bulk dispersed liquid].

The excess pressures in the drops, relative to that in the interstitial continuous phase, p_b , are often referred to as their *capillary pressures*, p_c . For example,

$$(p_c)_1 = p_1 - p_b = \sigma c_1 \quad (7)$$

It is clear that, in general, the capillary pressure varies from drop to drop.

When Eqs. (3) are combined with Eqs. (5), the following relationships between the curvatures of the films and those of the Plateau border walls are obtained:

$$\begin{aligned} 2C_{12} &= c_1 - c_2 \\ 2C_{23} &= c_2 - c_3 \\ 2C_{31} &= c_3 - c_1 \end{aligned} \quad (8)$$

For each film to be stable, it must be able to develop an internal, repulsive *disjoining pressure* Π_d to counteract the capillary suction acting at the film–Plateau border junction. At equilibrium, it can be readily shown

from the above that

$$\begin{aligned}
 (\Pi_d)_{12} &= \frac{\sigma(c_1 + c_2)}{2} \\
 (\Pi_d)_{23} &= \frac{\sigma(c_2 + c_3)}{2} \\
 (\Pi_d)_{31} &= \frac{\sigma(c_3 + c_1)}{2}
 \end{aligned} \tag{9}$$

Thus, the disjoining pressures in three confluent films are, in general, unequal. It turns out that the difference in the disjoining pressures in two of the films is defined by the curvature of the third film. For example, from Eqs. (9) and (8),

$$(\Pi_d)_{31} - (\Pi_d)_{23} = \frac{\sigma(c_1 - c_2)}{2} = \sigma C_{12} \tag{10}$$

[The inequality of the disjoining pressures implies that the films may have slightly different equilibrium thicknesses and tensions. In extreme cases (30), this may lead to sensible deviations from Plateau’s first law of foam structure, stated below.]

As the volume fraction approaches unity, the linear Plateau border shrinks into a line. In this “dry-foam” limit, mechanical equilibrium demands that the three films—of presumed equal tensions—meet pairwise at angles of 120° along this line (Plateau’s first law of foam structure). However, even when the Plateau border is finite and the films do not really intersect, the principle may well hold when applied to the virtual line of intersection that is obtained when the films, while maintaining their curvatures, are extrapolated into the border (dashed lines in Fig. 1b). A rigorous proof has been published by Bolton and Weaire (31) for two-dimensional (2D) foams, in which the Plateau borders are rectilinear. To our knowledge, no proof has yet been presented for the more general case of curvilinear borders in three-dimensional (3D) space. In fact, because the Plateau border can be viewed as a line with a line tension (32), this broader statement of Plateau’s first law may *not* strictly apply when the border has some finite longitudinal curvature.

A *tetrahedral* Plateau border is formed by the confluence of four linear Plateau borders (Fig. 1a). It fills the gap between the rounded corners of four adjoining polyhedral drops. The pressure in the tetrahedral border is, of course, equal to that in each of the outgoing linear borders, which sets the curvature of each of its four bounding walls. In the dry-foam limit ($\phi \rightarrow 1$), the tetrahedral border reduces to a point (“vertex” or “node”),

where the four linear borders meet pairwise at the angle of $\cos^{-1}(-1/3) = 109.47^\circ$ (Plateau's second law of foam structure). The principle probably remains valid for finite borders, when applied to the point where the four virtual lines of film intersection (see Fig. 1) meet upon extension into the tetrahedral border.

IV. OVERALL STRUCTURE AND OSMOTIC PRESSURE

Having described the structural elements of foams approaching the dry-foam limit ($\phi \rightarrow 1$), it is still a daunting task to describe the structure and properties of the system as a whole. The task is even more difficult for systems in which ϕ_0 is exceeded, but the polyhedral regime has not yet been reached. In this case, the drops have exceedingly complex shapes, and linear and tetrahedral Plateau borders, as defined earlier, are not present. Much can be learned about the qualitative behavior by considering *2D model systems*, in which the drops do not start out as spheres but as parallel circular cylinders and tetrahedral plateau borders do not arise. We shall first consider the particularly simple, perfectly ordered monodisperse case, with a subsequent gradual increase in complexity.

[Lest the reader think that 2D foams are just figments of the imagination, it must be pointed out that they can be generated—or at least closely approximated—by squeezing a 3D foam between two narrowly spaced, wetted, transparent plates (2,33–37). Structurally, even closer realizations may be obtained in phase-coexistence regions of insoluble monolayers of surface-active molecules at the air–water interface (38), where the role of surface tension is taken over by the line tension at the phase boundaries.]

A. Monodisperse, Perfectly Ordered 2D System

Such a system has been discussed in detail in Ref. 39. In the absence of gravity, the circular cylinders of radius R arrange in hexagonal packing (Fig. 2a) at a volume fraction $\phi_0 = \pi/2\sqrt{3} = 0.9069$. In cross section, each circular drop can be thought to be contained within a regular hexagon of side length $a_0 = 2R/\sqrt{3}$. As the volume fraction is increased, the drop is flattened against its six neighbors to form a hexagon of side length a ($< a_0$) but with rounded corners described by circular arcs of radius r (Fig. 2b). At constant drop volume, one finds

$$\frac{r}{R} = \left(\frac{\phi_0}{1 - \phi_0} \right)^{1/2} \left(\frac{1 - \phi}{\phi} \right)^{1/2} \quad (11)$$

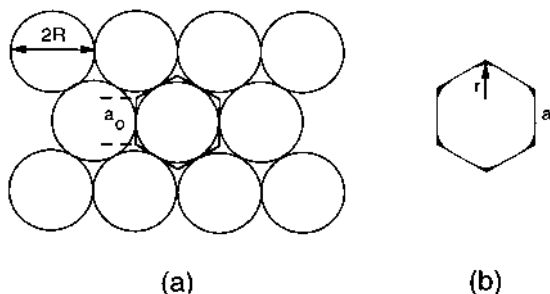


Figure 2 (a) Uncompressed cylindrical drops in hexagonal close packing ($\phi = \phi_0 = 0.9069$); (b) compressed drop ($0.9069 < \phi < 1$).

The capillary pressure in each drop is given by $p_c = \sigma/r$ or, when scaled by the initial capillary pressure $(p_c)_0 = \sigma/R$, by

$$\tilde{p}_c = p_c / (p_c)_0 = R/r \quad (12)$$

In the above process, the surface area of each drop, per unit of length, increases from $S_0 = 2\pi R$ to $S = 6(a - 2r/\sqrt{3}) + 2\pi r$, which, at constant drop volume, can be shown to lead to

$$\frac{S}{S_0} = \frac{1}{(\phi_0\phi)^{1/2}} [1 - (1 - \phi_0)^{1/2}(1 - \phi)^{1/2}] \quad (13)$$

This function has been plotted in Fig. 3. In the limit of $\phi = 1$, the scaled surface area reaches a maximum that is given by

$$\frac{S_1}{S_0} = \frac{1}{\phi_0^{1/2}} = 1.0501 \quad (14)$$

The scaled surface area and its variation with ϕ are of crucial importance in the definition and evaluation of the *osmotic pressure*, Π , of a foam or emulsion. We introduced the concept in Ref. 39, where it was referred to as the “compressive pressure,” P . It has turned out to be an extremely fruitful concept (24,29,40). The term “osmotic” was chosen, with some hesitation, because of the operational similarity with the more familiar usage in solutions. In foams and emulsions, the role of the solute molecules is played by the drops or bubbles; that of the solvent is played by the continuous phase, although it must be remembered that the nature of the interactions is entirely different. Thus, the osmotic pressure is defined as the pressure that needs to be applied to a semipermeable, freely movable

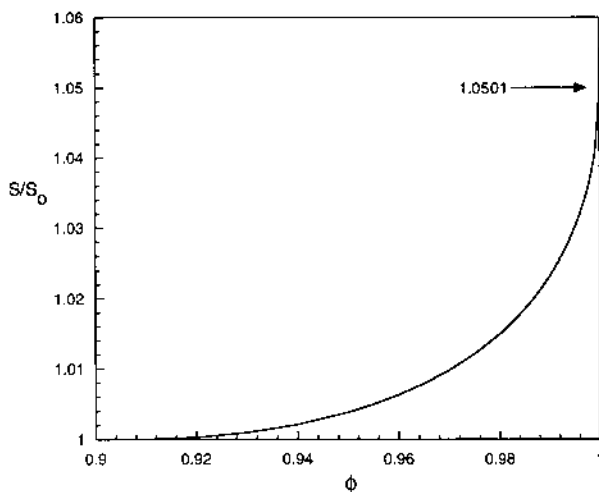


Figure 3 Scaled surface area, S/S_0 , for monodisperse 2D drops as a function of volume fraction.

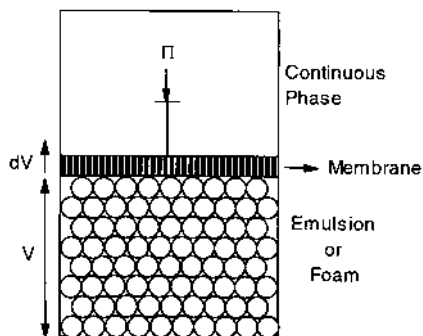


Figure 4 Semipermeable membrane separating dispersion from continuous phase; pressure to prevent additional continuous phase from entering the dispersion is the “osmotic” pressure, Π . [From Ref. 40. Copyright (1986) American Chemical Society.]

membrane, separating a fluid–fluid dispersion from its continuous phase, to prevent the latter from entering the former and to thereby reduce the augmented surface free energy (Fig. 4). The membrane is permeable to all of the components of the continuous phase but not to the drops or bubbles. As we wish to postpone discussion of compressibility effects in foams until later, we assume that the total volume (and therefore the volume of the dispersed phase) is held constant.

As long as the membrane is located high up in the box in Fig. 4, the emulsion or foam may be characterized by $\phi < \phi_0$ and $\Pi = 0$. As the membrane moves down, a point is reached where $\phi = \phi_0$. Any further downward movement requires work against a finite pressure Π , reflecting the increase in the total surface area as the drops are deformed; that is,

$$-\Pi dV = -\Pi dV_2 = \sigma dS \quad (\text{constant } V_1) \quad (15)$$

where V is the dispersion volume, V_1 is the volume of the dispersed phase, V_2 is the volume of the continuous phase in the dispersion, and σ is assumed to be constant. Because $V = V_1 + V_2$ and $\phi = V_1/V$, Eq. (15) leads to the completely general expression

$$\Pi = \sigma \phi^2 \frac{d(S/V_1)}{d\phi} = \sigma \phi^2 \frac{S_0}{V_1} \frac{d(S/S_0)}{d\phi} \quad (16)$$

where S/V_1 is the surface area per unit volume of the dispersed phase. Alternatively, as shown in Ref. 29, Π may be equated to the pressure difference between an ambient atmosphere and the continuous phase in the dispersion, or from Eq. (6):

$$\Pi = P - p_b = \sigma_c |C_l| \quad (17)$$

For yet a third useful way to express Π , see Refs. 24, 29, and 40.

For the special case of a monodisperse 2D system,

$$\frac{S_0}{V_1} = \frac{2}{R} \quad (18)$$

which, when combined with Eqs. (16) and (13), results in

$$\Pi = \frac{\sigma}{R} \left(\frac{\phi}{\phi_0} \right)^{1/2} \left[\left(\frac{1 - \phi_0}{1 - \phi} \right)^{1/2} - 1 \right] \quad (19)$$

or, in reduced form,

$$\tilde{\Pi} \equiv \frac{\Pi}{\sigma/R} = \frac{\Pi}{(p_c)_0} = \left(\frac{\phi}{\phi_0} \right)^{1/2} \left[\left(\frac{1 - \phi_0}{1 - \phi} \right)^{1/2} - 1 \right] \quad (20)$$

where $\phi_0 = 0.9069$. Figure 5 shows the dependence of $\tilde{\Pi}$ on ϕ .

The suggestion has been made (Exerowa, personal communication, 1990), since withdrawn (20,41), that Π and p_c are really identical. It is

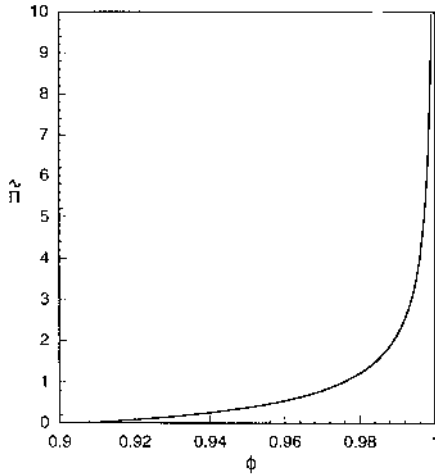


Figure 5 Reduced osmotic pressure as a function of ϕ for a perfectly ordered 2D system.

clear from the above that this is not so. In fact, examination of Eqs. (20), (11), and (12) shows that, at least for this simple model system,

$$\tilde{p}_c - \tilde{\Pi} = \left(\frac{\phi}{\phi_0}\right)^{1/2} \quad (21)$$

At $\phi = \phi_0$,

$$\tilde{p}_c - \tilde{\Pi} = 1 \quad (22)$$

At the upper limit of $\phi = 1$,

$$\tilde{p}_c - \tilde{\Pi} = \phi_0^{-1/2} = \frac{S_1}{S_0} = 1.0501 \quad (23)$$

Both \tilde{p}_c and $\tilde{\Pi}$ tend to infinity in this limit, but the *relative* difference between them tends to zero. This is the regime of concern in much of the interesting work of Exerowa et al. (e.g., Refs. 42 and 43), where the difference between the capillary and osmotic pressures may therefore, indeed, be safely ignored (41). However, this is not so in general and we shall demonstrate in Sect. V that $\tilde{\Pi}$ is a much more useful and informative parameter than \tilde{p}_c .

Before leaving this topic, it should be mentioned that modifications of most of the above expressions have been derived to take account of finite film thickness, finite contact angle at the film–Plateau border junction, or

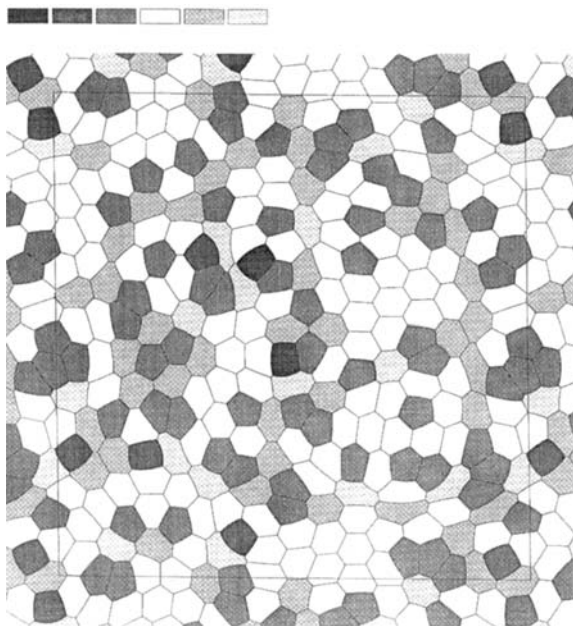


Figure 6 Topologically disordered, but volumetrically monodisperse 2D system ($\phi = 1$) with periodic boundaries; each shade corresponds to drops with a certain number of sides (e.g., the unshaded drops all have six sides). (Courtesy of T. Herdtle and A. M. Kraynik.)

both (39). Finally, it must be realized that a monodisperse 2D system does not necessarily pack in the perfectly ordered, hexagonal state depicted in Fig. 2. Herdtle et al. (personal communication, 1993) have constructed highly disordered, yet monodisperse 2D dry foams with periodic boundaries (Fig. 6), in which all films meet at angles of 120° and all film curvatures satisfy Eq. (4). In a sense, these systems are monodisperse only in a *volumetric* sense, but are *topologically* disordered or “polydisperse.” They are equilibrium structures, whose surface energy, although at a *local* minimum, must be higher than that of the perfectly ordered hexagonal system. Because the bubble pressures are not the same, such a system is bound to coarsen, thereby reducing its total surface energy. In practice, disorder of this type may be imposed by the finiteness of any system with bounding walls. If the walls are wetted by the continuous phase, then the outer films must be directed normal to the walls, which is generally incompatible with a perfectly ordered internal structure. As we shall see, this complication arises in 3D foams as well.

B. Polydisperse 2D Systems

In the last decade or so, much progress has been made toward a more complete understanding of these disordered structures. Most work relies on the computer generation of disordered (volumetrically) polydisperse structures with periodic boundary conditions, in which the film angles and curvatures obey the rules set forth in Sect. III. For a recent review, see Ref. 33. An example, taken from Ref. 44, is shown in Fig. 7. The structure contains many bubbles that are not hexagons, but it is readily proven that the *average* number of sides is still six (44). Simpler and very special types of (volumetric) polydispersity and disorder have been considered by Khan and Armstrong (45) and Kraynik et al. (46). In these cases, illustrated in Fig. 8, the topology is preserved. All bubbles are still hexagons and all films remain flat; the bubbles, therefore, do not coarsen with time. The first system (Fig. 8a) is simply bimodal and is obtained by increasing or decreasing the height of all bubbles in a given row. The second system (Fig. 8b) is much more disordered and can be generated from the monodisperse system by randomly increasing (or decreasing) each bubble area, as illustrated in Fig. 9, with the limitation that no vertices ever touch or cross over, lest Plateau's first law be violated and resultant (so-called T1) rearrangements lead to a much more complex structure. The total surface area is not affected by such transformations, so that, as in the monodisperse case,

$$\frac{S_1}{S_0} = 1.0501 \quad (24)$$

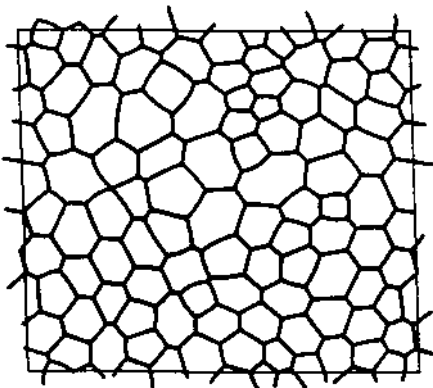


Figure 7 Computer-generated, topologically disordered and volumetrically polydisperse 2D system ($\phi=1$) with periodic boundaries. (From Ref. 44, with permission from Taylor & Francis Ltd.)

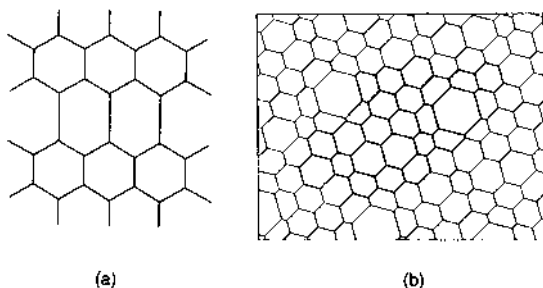


Figure 8 (a) Simplest case of volumetrically bimodal 2D system; (b) more highly disordered, volumetrically polydisperse hexagonal 2D system ($\phi = 1$). The cluster of darkly outlined drops forms the repeating unit. (Courtesy of A. M. Kraynik. Similar structures appear in Ref. 46.) In both cases, the system is topologically “monodisperse.”

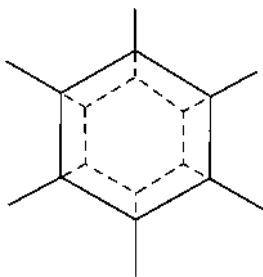


Figure 9 Recipe for creating a volumetrically polydisperse (but topologically monodisperse) hexagonal system from perfectly ordered 2D system; total surface energy remains unchanged.

This is not necessarily true for the more general structures such as that in Fig. 7, which is both volumetrically and topologically polydisperse. Unfortunately, although presumably available as a result of the numerical simulations, the value of S_1/S_0 and how it varies with the details of the size distribution appear not to have been reported for these cases.

Starting from a dry-foam system as in Fig. 7, the volume fraction can be lowered by “decorating” each vertex with a Plateau border, whose wall curvatures obey the rules set forth in Sect. III (31). As the volume fraction is lowered by increasing the size of the Plateau borders, a point is soon reached where adjacent Plateau borders “touch” and subsequently merge into single four-sided borders. Bolton and Weaire (47) have followed this process down

to the volume fraction ϕ_c , where all bubbles are spherical and structural rigidity is lost. This is perhaps the most satisfactory definition of ϕ_0 . Their finding suggests that, for that particular system, ϕ_c equaled 0.84 (not 0.9069), which happens to be close to the random packing density of (monodisperse) circular disks. Using similar computer simulations, Hutzler and Weaire (48) calculated the osmotic pressure and found it to obey Eq. (19) closely in the “drier” regime. It started to deviate at lower volume fractions and did not reach zero until ϕ dropped to about 0.82, which is close to ϕ at the rigidity loss transition.

C. Monodisperse 3D Systems

Ideally, uniform spheres arrange in “hexagonal close” packing, which is face-centered cubic (fcc), at $\phi_0 = \pi\sqrt{2}/6 = 0.7405$. The role of the circumscribing hexagon in monodisperse 2D systems is taken over by the rhombic dodecahedron (Fig. 10). As the volume fraction is raised, each drop flattens against its 12 neighbors. This process has been described by Lissant (4,5), who considered the drop to be transformed into a truncated sphere and each

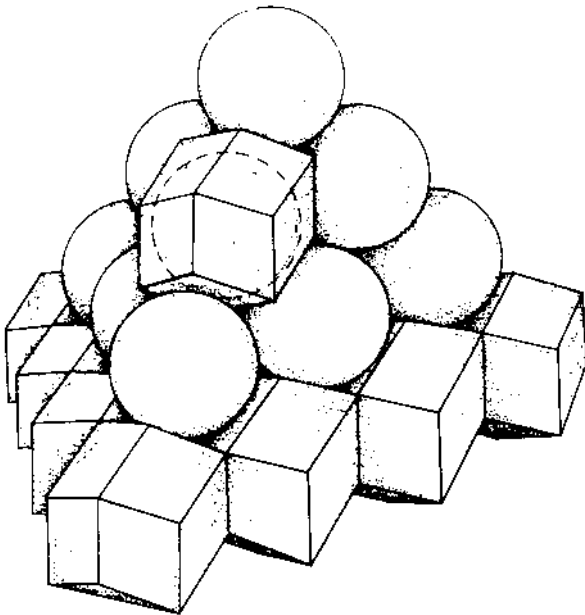


Figure 10 Spheres in hexagonal close packing (fcc), each occupying a rhombic dodecahedron. (From Ref. 4, with permission from Academic Press.)

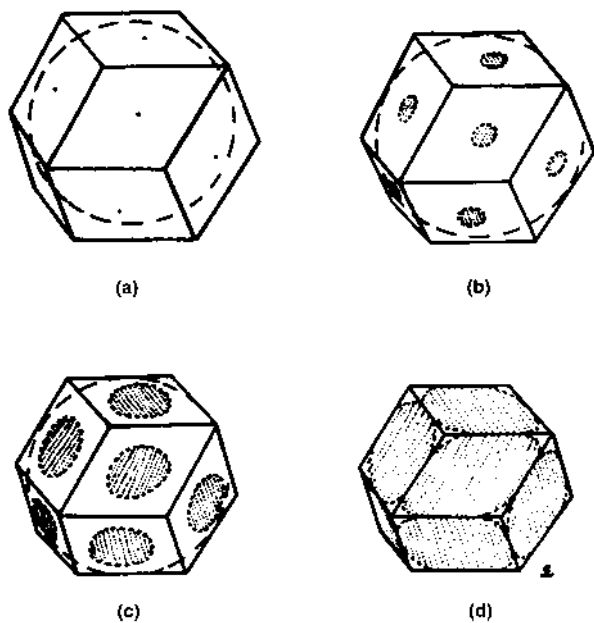


Figure 11 Each drop flattens against its neighbors as the volume fraction increases; a stable thin film of continuous phase separates neighboring drops. (From Ref. 4, with permission from Academic Press.)

film to be circular, at least until it reaches the sides of the diamond faces (Fig. 11). This is incompatible with a zero contact angle at the film edge. Moreover, at constant drop volume, this model would imply *decreasing* capillary (and osmotic) pressure with increasing ϕ , which is clearly inconsistent. In reality, the problem is much more complicated; the drop cannot remain spherical and the films must be noncircular. Using Brakke's now famous "Surface Evolver" computer software (49), Kraynik and Reinelt (50), and Lacasse et al. (51) have correctly and accurately solved this problem for this and other structures (discussed later in this subsection).

As suggested already by Lissant (4,5), the packing is likely to change above some critical value of ϕ . It is clear that if the dodecahedral packing were to persist up to $\phi=1$, Plateau's second law would be violated at 6 of the 14 corners of the polyhedron, because 8 linear borders would converge there, rather than the mandatory 4. Lissant proposed that the structure changes to a body-centered cubic (bcc) packing of planar tetrakaidecahedra (truncated octahedra; see Fig. 12a). However, such a structure satisfies neither of Plateau's laws. In this dry-foam regime, Kelvin's "minimal

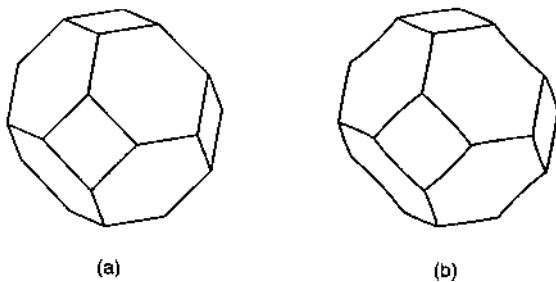


Figure 12 (a) Planar tetrakaidecahedron (or truncated octahedron); (b) Kelvin's minimal tetrakaidecahedron (bcc).

tetrakaidecahedron” (Fig. 12b), which is obtained by slight distortion of its planar counterpart, solves this problem and has long been considered as the most satisfactory candidate for the drop shape. It has 6 planar quadrilateral faces, 8 nonplanar hexagonal faces of zero mean curvature, and 36 identical curved edges. In a space-filling ensemble of such polyhedra, Plateau’s first and second laws are fully satisfied. Kelvin derived approximate expressions for the shape of the hexagons and the sides (52–54). Based on that model, Princen and Levinson (55) calculated the length of the sides and the surface areas of the quadrilateral and hexagonal faces, relative to those of the parent planar tetrakaidecahedron of the same volume. They arrived at the following result for the increase in surface area as a spherical drop transforms into a Kelvin tetrakaidecahedron of the same volume:

$$\frac{S_1}{S_0} = 1.0970 \quad (25)$$

(This compares to values of 1.0990 for the planar tetrakaidecahedron, 1.1053 for the rhombic dodecahedron, and 1.0984 for the regular pentagonal dodecahedron. The latter—although often considered as a unit cell in foam modeling—is not really a viable candidate either, as it not only violates Plateau’s laws but is also not space filling.)

More recently, Reinelt and Kraynik (56) have carried out more exact numerical calculations on the Kelvin cell, leading to the slightly higher value of

$$\frac{S_1}{S_0} = 1.0972 \quad (26)$$

Kelvin’s polyhedron would indeed represent the ideal drop shape in the dry-foam limit by effecting, in Kelvin’s own words, “a division of space with

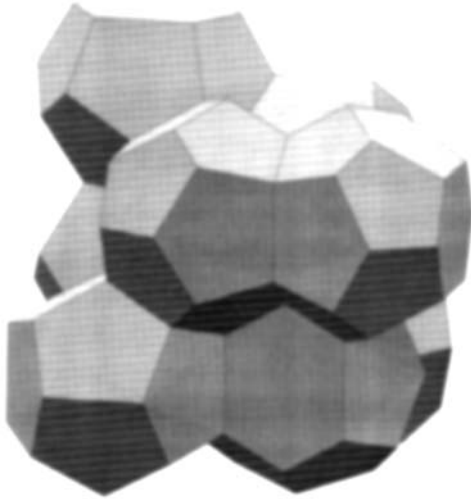


Figure 13 Unit cell in Weaire–Phelan structure, containing 2 pentagonal dodecahedra and 6 tetrakaidecahedra, each having 12 pentagonal and 2 hexagonal faces. (Courtesy of A. M. Kraynik.)

minimum partitional area,” if he had added the proviso that this division is to be accomplished with identical cells. It has recently been proven by Weaire and Phelan (57) that at least one structure of even lower energy exists, if this restriction is lifted. The Weaire–Phelan structure (Fig. 13), whose surface area is about 0.34% lower than that of Kelvin (i.e., $S_1/S_0 = 1.0936$), has repeating units that contain 8 equal-volume cells: 2 identical pentagonal dodecahedra and 6 identical tetrakaidecahedra that each have 12 pentagonal and 2 hexagonal faces. The pressure in the dodecahedra is slightly higher than that in the tetrakaidecahedra. Perhaps surprisingly, neither the Kelvin nor the Weaire–Phelan structure is rarely, if ever, encountered in actual monodisperse foams (3). The reason for this may lie in small deviations from monodispersity or, more likely, in the disturbing effects of the container walls, as alluded to already in connection with 2D foams. Alternatively, as the continuous phase is removed from between the initially spherical drops in fcc packing, slight irregularities in this drainage process may force the system to get trapped in a less-ordered structure that may be at a local surface area minimum but is separated from the lower-energy Kelvin and Weaire–Phelan structures by a significant barrier [cf. the difficulty one encounters in trying to build a 15-bubble cluster that has a Kelvin polyhedron at its center (58)].

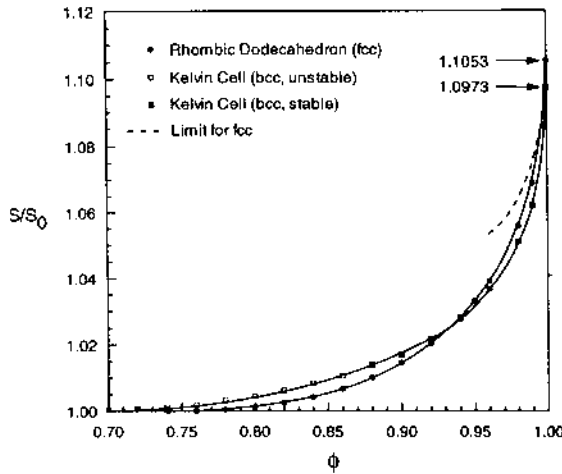


Figure 14 Scaled surface areas as a function of volume fraction for the rhombic dodecahedral (fcc) and Kelvin structures (bcc). (From data kindly provided by A. M. Kraynik and D. A. Reinelt.)

Kraynik and Reinelt (50) and Lacasse et al. (51) have accurately computed the changes in surface area as a drop transforms from a sphere into a regular dodecahedron (fcc) or a Kelvin cell (bcc) with increasing volume fraction while maintaining zero contact angle. Expressed in terms of S/S_0 , the results are shown in Fig. 14. The Kelvin structure is internally unstable below $\phi \approx 0.87$. The results further indicate that the Kelvin cell becomes the more stable structure above $\phi \approx 0.93$. Also indicated is the limiting law for $\phi \rightarrow 1$ for the dodecahedron. In that regime, linear Plateau borders of constant cross section run along the edges of the polyhedron. Their volumes and surface areas can be evaluated as a function of ϕ , whereas the volumes and surface areas of the tetrahedral borders become negligible. For the rhombic dodecahedron (24), this leads to

$$\frac{S}{S_0} = 0.0686[1 - 1.892(1 - \phi^{1/2})]^3 + 1.0367 \quad (\phi \rightarrow 1)$$

Kraynik and Reinelt (50) also evaluated the all-important osmotic pressure $\Pi(\phi)$, which, for 3D structures, is given by [cf. Eq. (16)]

$$\Pi = \sigma \phi^2 \frac{S_0}{V_1} \frac{d(S/S_0)}{d\phi} = \frac{3\sigma \phi^2}{R} \frac{d(S/S_0)}{d\phi}$$

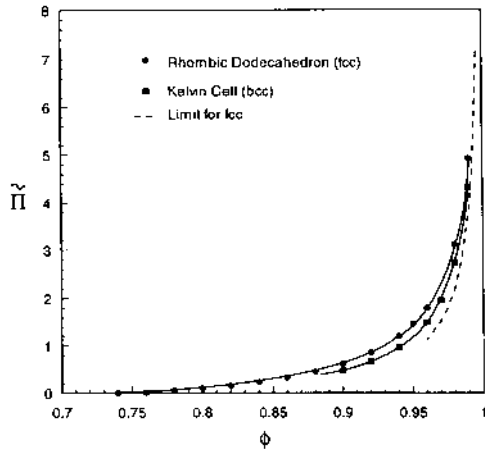


Figure 15 Reduced osmotic pressure as a function of volume fraction for the rhombic dodecahedral and Kelvin structures. (From data kindly provided by A. M. Kraynik and D. A. Reinelt.)

where R is the radius of the initially spherical drops, or

$$\tilde{\Pi} \equiv \frac{\Pi}{\sigma/R} = 3\phi^2 \frac{d(S/S_0)}{d\phi} \quad (27)$$

For the dodecahedron, the appropriate limiting law for $\phi \rightarrow 1$ is given (24) by

$$\tilde{\Pi} = \frac{\Pi}{\sigma/R} = 0.5842\phi^{1/3} \frac{[1 - 1.892(1 - \phi)^{1/2}]^2}{(1 - \phi)^{1/2}} \quad (\phi \rightarrow 1) \quad (28)$$

Figure 15 shows $\tilde{\Pi}(\phi)$ for the dodecahedron and Kelvin cell.

Detailed numerical calculations have been carried out by Bohlen et al. (59) for the transition of monodisperse spheres in simple *cubic* packing ($\phi_0 = 0.5236$) to cubes ($\phi = 1$), for both zero and finite contact angles. Unfortunately, although the results are interesting, this kind of packing is not realistic for foams and emulsions and will not be discussed further.

D. Polydisperse 3D Systems

This is, of course, the system of greatest interest from a practical point of view. The detailed structure is exceedingly complex. As mentioned earlier,

even the value of ϕ_0 is not precisely defined and is expected to depend somewhat on the details of the size distribution. Nevertheless, there is clear experimental evidence (23,24) that ϕ_0 is close to—or slightly smaller than—0.7405 for “typical,” polydisperse, unimodal emulsions.

In the dry-foam limit, each polyhedral drop must satisfy Euler’s formula; that is,

$$v - e + f = 2 \quad (29)$$

where v is the number of vertices, e is the number of edges, and f is the number of faces. For an infinite number of space-filling polyhedra that are subject to Plateau’s rules, a number of statistical relationships can be derived from Eq. (29) (60–62). Perhaps the most interesting of these is

$$\langle f \rangle = \frac{12}{6 - \langle e \rangle} \quad (30)$$

where $\langle f \rangle$ is the average number of faces per cell and $\langle e \rangle$ is the average number of edges per face. Equation (30) is consistent with what is expected for a monodisperse “Kelvin foam,” where $\langle f \rangle = f = 14$ and $\langle e \rangle = (6 \times 4 + 8 \times 6)/14 = 5.143$, or a Weaire–Phelan structure, where $\langle f \rangle = (2 \times 12 + 6 \times 14)/8 = 13.5$ and $\langle e \rangle = [2 \times 12 \times 5 + 6 \times (12 \times 5 + 2 \times 6)]/108 = 5.111$. As mentioned earlier, Matzke (3) found that, in a real, supposedly monodisperse foam, Kelvin’s polyhedra did not occur and that pentagonal faces were predominant. He found that $\langle f \rangle = 13.70$ and $\langle e \rangle = 5.124$, which is, again, consistent with Eq. (30). For a real polydisperse dry foam, Monnereau and Vignes-Adler (63) found $\langle f \rangle = 13.39 \pm 0.05$ and $\langle e \rangle = 5.11$, again in close agreement with Eq. (30). These authors did not encounter any Kelvin cell (or Weaire–Phelan structure) either.

For $\phi_0 < \phi < 1$, the drops go through a complex transition from spheres to pure polyhedra. In this most general system, the osmotic pressure is given by

$$\Pi(\phi) = \sigma \phi^2 \frac{S_0}{V_1} \frac{d(S/S_0)}{d\phi} = \frac{3\sigma \phi^2}{R_{32}} \frac{d(S/S_0)}{d\phi} \quad (31)$$

where R_{32} is the surface/volume or Sauter mean radius of the initially spherical drops:

$$R_{32} \equiv \frac{\sum n_i R_i^3}{\sum n_i R_i^2} = \frac{3V_1}{S_0} \quad (32)$$

Although R_{32} can be readily measured for any practical system, the complex geometry does not allow the evaluation of $S(\phi)/S_0$ and $\Pi(\phi)$ from first principles. Instead, in the next section, we shall show how these and other important functions can be derived from experiment.

V. UTILITY AND EXPERIMENTAL EVALUATION OF THE OSMOTIC PRESSURE

We have repeatedly emphasized the importance and utility of the osmotic pressure Π of foams and concentrated emulsions. Once known as a function of ϕ , it may be used to quantitatively link and predict a large number of other important properties. Some of these are listed in this section. In addition, these considerations lead to a convenient method for evaluating $\Pi(\phi)$ experimentally (see Sec. V.D).

A. Motion of Continuous Phase Between Different Systems in Contact

Let two concentrated dispersions with the same type of continuous phase [e.g., an aqueous foam and an oil-in-water emulsion, or two different o/w emulsions] be brought into contact, either directly or via a freely movable semipermeable membrane. If the osmotic pressures are unequal (e.g., as a result of differences in the volume fractions, mean drop size, interfacial tension, or combinations thereof), it is obvious that the (common) continuous phase will flow from the dispersion with the lower osmotic pressure into that with the higher osmotic pressure until the two pressures are equalized. The final volumes and volume fractions of the two dispersions may be predicted in a straightforward manner, once $\tilde{\Pi}(\phi)$ is known. It is important to point out that equality of the (mean) *capillary pressures* does not necessarily rule out flow nor does their inequality imply it.

B. Vapor Pressures of Continuous and Dispersed Phases

It can be shown (29) that the vapor pressure, p_v^c , of the continuous phase is reduced to below that of the bulk continuous phase, $(p_v^c)_0$, according to

$$p_v^c = (p_v^c)_0 \exp\left(\frac{-\Pi \bar{V}_2}{\Re T}\right) \quad (33)$$

where \bar{V}_2 is the partial molar volume of the solvent, \Re is the gas constant, and T is the absolute temperature.

Similarly, the vapor pressure of the dispersed phase, p^d , in a concentrated emulsion can be related to that of the bulk dispersed phase, $(p_v^d)_0$ by

$$p_v^d \approx (p_v^d)_0 \exp\left(\frac{2\sigma \bar{V}_1 S}{R_{32} \mathfrak{R} T S_0}\right) \quad (34)$$

where σ is the interfacial tension, R_{32} is the Sauter mean drop radius, \bar{V}_1 is the molar volume of the dispersed liquid, and S/S_0 is the relative increase in surface area at the volume fraction ϕ . For $\phi < \phi_0$, where $S/S_0=1$, we recover a variant of Kelvin's equation; for $\phi > \phi_0$, the increased vapor pressure is augmented further by the appearance of the factor S/S_0 in the exponent, with S/S_0 being related to $\Pi(\phi)$ through Eq. (31).

C. Gradient in ϕ in Gravitational Field

So far, we have assumed that gravity is absent or negligible, so that the volume fraction is uniform throughout the system. In gravity, however, a sufficiently tall column will develop a significant gradient in ϕ (24). Even if each individual drop is small enough to be essentially unaffected by the field (i.e., when the Bond number is very small), the combined buoyant force of the underlying drops causes increasing drop deformation (and volume fraction) in the higher regions (Fig. 16). At the boundary between the dispersion and the bulk continuous phase, where $z=0$, we have $\phi=\phi_0$, and the drops are purely spherical. At higher z , they increasingly deform until, as $z \rightarrow \infty$, they acquire a purely polyhedral shape and $\phi \rightarrow 1$. It is

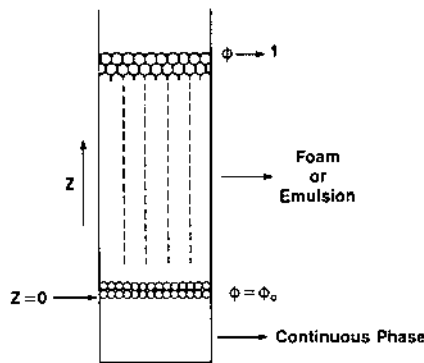


Figure 16 Transition from spherical to polyhedral drops in vertical column. [From Ref. 40. Copyright (1986) American Chemical Society.]

clear that, at any level, the combined buoyant force of all underlying drops per unit area must equal the local osmotic pressure:

$$\Pi(\phi) = \Delta\rho g \int_0^z \phi dz \quad (35)$$

or

$$\tilde{\Pi}(\phi) = \frac{\Delta\rho g R_{32}}{\sigma} \int_0^z \phi(z) dz = \int_0^{\tilde{z}} \phi(\tilde{z}) d\tilde{z} \quad (36)$$

where $\Delta\rho$ is the density difference between the phases, g is the acceleration due to gravity, $\tilde{\Pi}(\phi)$ is the reduced osmotic pressure

$$\tilde{\Pi}(\phi) = \frac{\Pi(\phi)}{\sigma/R_{32}} \quad (37)$$

and \tilde{z} is the reduced height

$$\tilde{z} \equiv \frac{R_{32}z}{a_c^2} \quad (38)$$

where $a_c = [\sigma/(\Delta\rho g)]^{1/2}$ is the capillary length.

In all of the above, it is assumed that there is no gravitational segregation by drop size, that is, the drop size distribution does not vary with height.

Thus, once $\tilde{\Pi}(\phi)$ is known, $\phi(\tilde{z})$ can be evaluated from Eq. (36) in the form

$$\tilde{z}(\phi) = \int_0^{\tilde{\Pi}} \frac{d\tilde{\Pi}(\phi)}{\phi} = \int_{\phi_0}^{\phi} \frac{1}{\phi} \left(\frac{d\tilde{\Pi}(\phi)}{d\phi} \right) d\phi \quad (39)$$

As mentioned earlier, the only system for which $\tilde{\Pi}(\phi)$ is known exactly is the monodisperse 2D system [cf. Eq. (16)]. When Eq. (39) is applied to this case, we find

$$\tilde{z}(\phi) = \frac{1}{(\phi_0\phi)^{1/2}} \left[1 + \left(\frac{1-\phi_0}{1-\phi} \right)^{1/2} (2\phi-1) \right] - 2 \quad (40)$$

where $\phi_0 = 0.9069$. This result has been obtained also by Pacetti (64). The volume fraction profile is shown in Fig. 17.

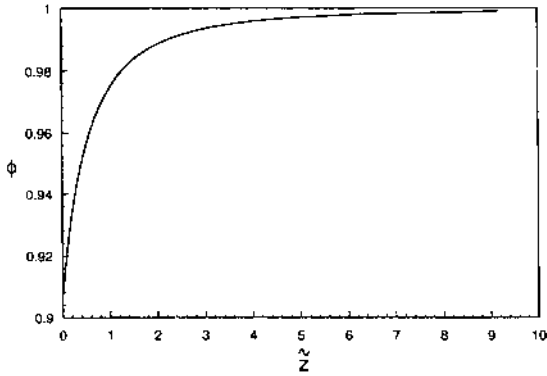


Figure 17 Volume fraction versus reduced height for perfectly ordered 2D case.

D. Experimental Determination of $\tilde{\Pi}(\phi)$ for Real Systems

From the above, it is clear that $\tilde{\Pi}(\phi)$ may be evaluated experimentally from Eq. (36) by determining the volume fraction as a function of height in an equilibrated (i.e., completely drained) dispersion column. This has been done very carefully for a typical, well-characterized polydisperse emulsion of paraffin oil in water (24). The emulsion had a Sauter mean drop radius of $R_{32} = 44.7 \mu\text{m}$, an interfacial tension of 7.33 mN/m , and a density difference of 0.144 g/cm^3 . The experimental profile $\phi(\tilde{z})$ is given in Fig. 18 and may be compared with that in Fig. 17 for the monodisperse 2D system. It could be numerically fitted to the following equations, covering three different ranges of ϕ :

“Low”-volume fraction ($0.715 < \phi < 0.90$ or $0 < \tilde{z} < 0.5$):

$$\tilde{z} = 0.237 \left(\frac{\phi - 0.715}{1 - \phi} \right) \quad (41)$$

or

$$\phi = \frac{\tilde{z} + 0.169}{\tilde{z} + 0.237} \quad (42)$$

This leads to

$$\tilde{\Pi}(\tilde{z}) = \tilde{z} - 0.068 \ln(\tilde{z} + 0.237) - 0.098 \quad (43)$$

which, upon substitution for \tilde{z} according to Eq. (41), leads to $\tilde{\Pi}(\phi)$. Equation (41) shows that $\phi = \phi_0 = 0.715$ at $\tilde{z} = 0$. This is one of our

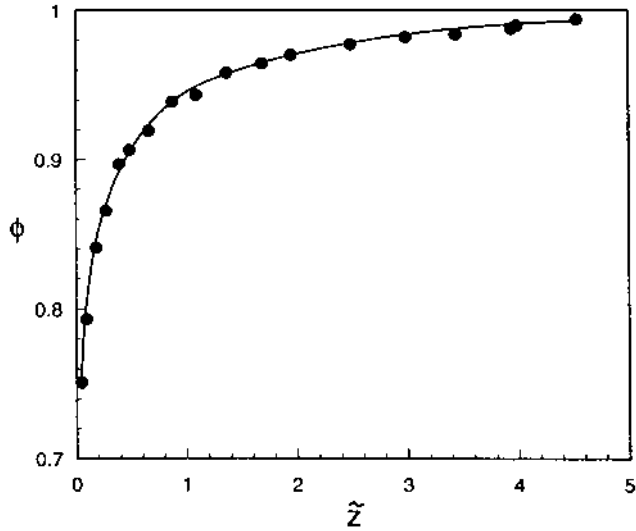


Figure 18 Experimental profile of volume fraction versus reduced height for typical polydisperse emulsion. [From Ref. 24. Copyright (1987) American Chemical Society.]

reasons for concluding that typical polydisperse systems pack slightly less tightly than ideally close-packed monodisperse systems, where $\phi_0 = 0.7405$.

Intermediate-volume fraction ($0.90 < \phi < 0.99$ or $0.5 < \tilde{z} < 4.0$):

$$\phi = 1.037[1 - (117.6\tilde{z} + 4.0)^{-1/2}] \quad (44)$$

and

$$\tilde{\Pi} = \frac{0.00819\phi^2}{(1 - 0.9639\phi)^2} \quad (45)$$

High-volume fraction ($0.99 < \phi < 1$ or $\tilde{z} > 4.0$):

$$\tilde{z} \approx \tilde{\Pi} = 0.5842 \frac{[1 - 1.892(1 - \phi)^{1/2}]^2}{(1 - \phi)^{1/2}} \quad (46)$$

which is the appropriate limiting solution for the polyhedral system.

Equations (42), (43), (45), and (46) describe the dependence of $\tilde{\Pi}$ on ϕ , as shown in Fig. 19. It may be compared with that for the monodisperse 2D

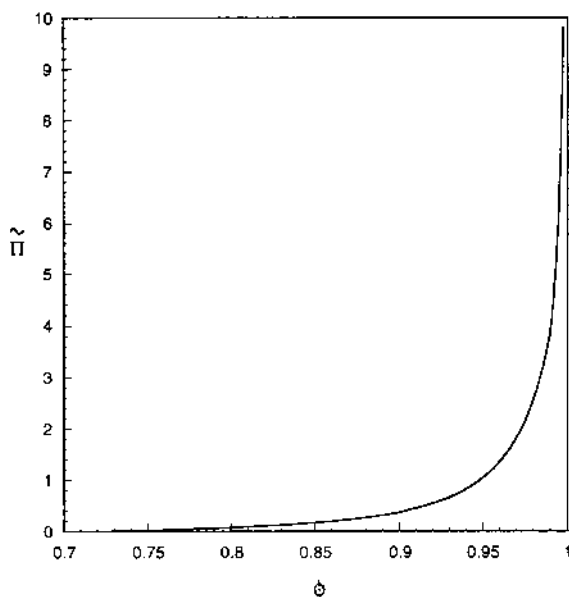


Figure 19 Reduced osmotic pressure as a function of volume fraction for typical polydisperse emulsion. [From Ref. 24. Copyright (1987) American Chemical Society.]

and 3D systems in Figs. 5 and 15, respectively. Close examination shows that the experimental osmotic pressure is consistently lower than those for the idealized structures in Fig. 15.

Even though these relationships were derived for one particular emulsion, its size distribution was “typical,” so that we believe that they can be applied with reasonable confidence in most practical situations. Nevertheless, more work remains to be done to elucidate the effect of the details of the size distribution. There is a particular need for the equivalent expressions for the *monodisperse* system, which would serve as a benchmark. Bibette’s (65) novel way of preparing emulsions of low polydispersity ($\pm 10\%$ in radius) has opened up experimentation along these lines. Unfortunately, the technique appears to be capable only of generating emulsions of extremely small drop size ($R < 1 \mu\text{m}$), which complicates matters in several ways. First, estimates of the effective volume fractions [cf. Eq. (1)] become questionable, unless detailed quantitative information is available on the equilibrium film thickness as a function of the apparent volume fraction (or capillary pressure). This is usually not the case, potentially leading to significant errors. Second, droplets of such small size are Brownian, which may lead to an entropic contribution to the osmotic

pressure, in addition to the energetic contribution considered so far. These and other factors may be responsible for some of the differences between the above results and those of Mason et al. (66), who measured $\Pi(\phi)$ for an oil-in-water “Bibette emulsion” of $R = 0.48 \mu\text{m}$. To cover the whole range of ϕ , they used three different ways to generate the osmotic pressure: gravitational compaction, centrifugation, and dialysis of the emulsion against the continuous phase containing various levels of dextran, a polymer to which the dialysis membrane is impermeable. The osmotic pressure was found to rise at an estimated effective ϕ of $(\phi_0)_e \approx 0.60$ (rather than 0.715). This is close to 0.64, the value for random close packing of uniform spheres. Up to $\phi_e = 0.80$, the data could be fitted well to

$$\tilde{\Pi} \propto \phi^2(\phi - 0.60) \quad (\phi < 0.80).$$

For $\phi > 0.80$, the results of the two studies appear to be quite consistent, in spite of the disparity in the degree of polydispersity of the emulsions employed. The apparent discrepancy at the lower volume fractions may be entirely due to the large difference in mean drop size, for the reasons cited earlier.

E. Gravitational Syneresis or Creaming

In the absence of gravity (or with fluids of matched densities), a perfectly stable emulsion or foam with $\phi > \phi_0$ will remain uniform and not “phase separate”, (i.e., it will not exude a bottom layer of continuous phase). In a gravitational (or centrifugal) field, such syneresis may occur, however, as a result of compaction in the upper region (assuming that we are dealing with a foam or o/w emulsion; the continuous phase would separate at the *top* in w/o emulsions). In a consumer product, such behavior could be detrimental, as it might suggest instability, breakdown, and limited shelf life, even though simple shaking would restore (temporary) uniformity. With the knowledge contained in the previous subsection, it is possible to predict exactly when such syneresis will in fact occur (67). For a container of constant cross section, the parameters of importance are the overall volume fraction, $\bar{\phi}$, and the reduced height of the sample, \tilde{H} , defined by

$$\tilde{H} \equiv \frac{HR_{32}}{a_c^2} = HR_{32} \Delta\rho \frac{g}{\sigma} \quad (47)$$

where H is the actual height of the sample. It is clear that, for any $\bar{\phi}$, there must be a critical reduced sample height, \tilde{H}_{cr} , above which syneresis will

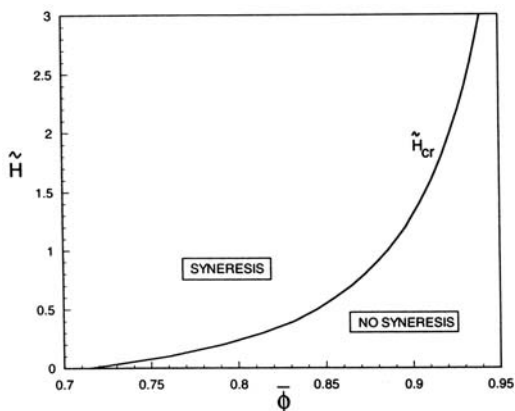


Figure 20 Critical sample height for occurrence of syneresis as a function of overall volume fraction.

occur and below which it will not. From a material balance and Eq. (36), it is readily shown that \tilde{H}_{cr} must obey the condition

$$\tilde{H}_{cr} = \frac{\tilde{\Pi}(\tilde{H}_{cr})}{\phi} \quad (48)$$

Figure 20 shows how the resulting $\tilde{H}-\bar{\phi}$ diagram is bisected by $\tilde{H}_{cr}(\bar{\phi})$. Reference 67 provides procedures for determining the height of the separated layer of continuous phase, if any, as well as the precise variation of ϕ with height in the sample. The method may be extended to containers with varying cross section (67). The following general conclusions may be drawn: (a) Everything else being equal, syneresis is less likely the higher the overall concentration of the dispersed phase, $\bar{\phi}$; of course, when $\bar{\phi} < \phi_0$, syneresis will *always* occur; (b) For given $\bar{\phi}$ ($> \phi_0$), the tendency toward syneresis is less pronounced the smaller \tilde{H} {i.e., for small drop size, high interfacial tension, small density difference, and small sample height [cf. Eq. (47)]}; (c) For a foam or typical o/w emulsion, the tendency toward syneresis is reduced if the container is shaped with its widest part at the bottom. The reverse is true for typical w/o emulsions.

F. Increase in Specific Surface Area with ϕ

We have seen that the osmotic pressure is directly linked to the scaled specific surface area, S/S_0 , as ϕ increases from ϕ_0 through Eq. (31). For the mono-disperse 2D system, S/S_0 is given by Eq. (13) and is plotted in Fig. 3.

To the extent that the real emulsion studied in Ref. 24 is representative of typical polydisperse 3D systems, one can derive S/S_0 from the expressions for $\bar{\Pi}(\phi)$ in Section V.D. The results (24) are as follows:

For $0.715 < \phi < 0.90$,

$$\frac{S}{S_0} = 1 + \frac{1}{3} \left[\frac{0.084}{\phi} - \frac{0.068}{\phi} \ln(1 - \phi) - 0.237 \right] \quad (49)$$

For $0.90 < \phi < 0.99$,

$$\frac{S}{S_0} = \frac{0.00283}{1 - 0.9639\phi} + 0.989 \quad (50)$$

For $0.99 < \phi < 1$,

$$\frac{S}{S_0} = 1.014 + 0.0686[1 - 1.892(1 - \phi)^{1/2}]^3 \quad (51)$$

The combined results are shown in Fig. 21, where it is seen that the transition from spheres to completely developed polyhedra is accompanied by an increase in surface area of 8.3%. As mentioned earlier, for the *monodisperse* case, one predicts an increase in surface area of 9.7% on the basis of

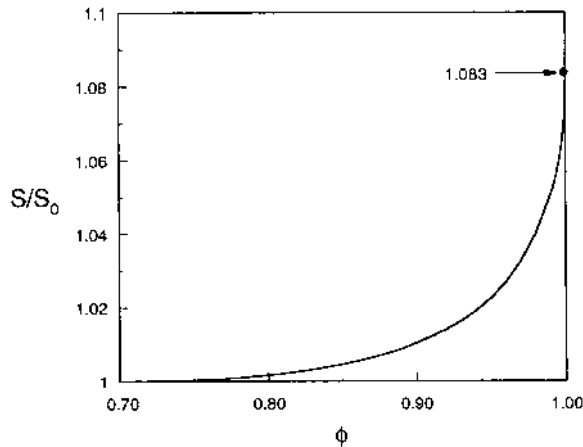


Figure 21 Scaled specific surface area as a function of volume fraction for typical polydisperse emulsion. [From Ref. 24. Copyright (1987) American Chemical Society.]

Kelvin's polyhedron as the ultimate drop shape, or 9.4% for the Weaire–Phelan structure. Polydispersity appears to give rise to an even somewhat *smaller* overall change in surface area. Recent computer simulations of various monodisperse and polydisperse structures by Kraynik et al. (68) confirm this result almost quantitatively.

G. Surface Area in Films Versus Total Surface Area

At any given volume fraction ϕ , a fraction S_f/S of the total surface area forms part of the films separating the droplets, and the remainder is still “free” in the Plateau borders ($S_f/S=0$ at $\phi=\phi_0$; $S_f/S=1$ at $\phi\rightarrow 1$). This parameter may play an important role in problems relating to the stability of, and mass transfer in, such systems. We have shown (29) that

$$\frac{S_f}{S} = \frac{S_1/S_0 f(\phi)}{S/S_0 \phi^{2/3}} \approx \frac{1.083 f(\phi)}{\phi^{2/3} S/S_0} \quad (52)$$

where S/S_0 is given by Fig. 21 and $f(\phi)$ is the fraction of a confining wall that is “contacted” by the flattened parts of the drops pushing against it, under the assumption that the wall is perfectly wetted by the continuous phase. This fraction, which varies from $f=0$ at ϕ_0 to $f=1$ at $\phi=1$, can be measured experimentally (69) and was found empirically to be given by

$$f(\phi) = 1 - \frac{3.20}{(\phi/(1-\phi) + 7.70)^{1/2}} \quad (53)$$

for $\phi_0 < \phi < 0.975$. (By solving for ϕ at $f=0$, we again obtain evidence that $\phi_0 \approx 0.72$ for real, polydisperse systems.) For $\phi > 0.975$, we expect that $f(\phi)$ is given, to a good approximation (40), by

$$f(\phi) = [1 - 1.892(1-\phi)^{1/2}]^2 \quad (54)$$

Combining Eqs. (53) and (54) with Eq. (52) leads to the approximate dependence of S_f/S on ϕ as shown in Fig. 22.

These are just some of the examples of where and how the osmotic pressure, or its related properties, can be used to define the overall equilibrium behavior of these complex fluids, even though their detailed microscopic structure may not be fully known. Other examples are presented in Section VI, where we describe the only properties that are unique to foams as a result of the compressibility of their dispersed phase.

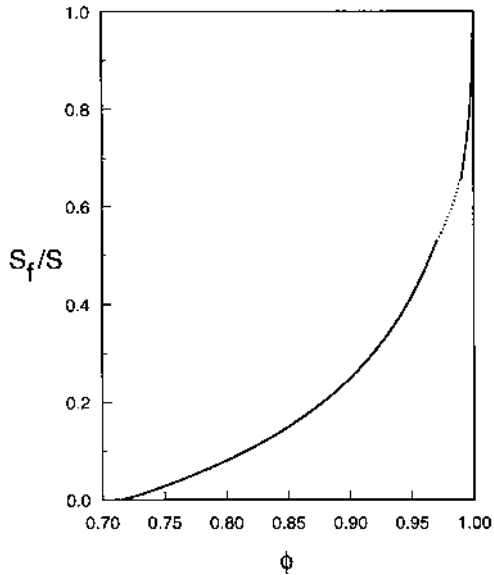


Figure 22 Fraction of total surface area contained in films as a function of volume fraction for typical polydisperse emulsion. Solid curve at right is limiting solution for fcc; the dashed curve connects it to the lower experimental region. [From Ref. 29. Copyright (1988) American Chemical Society.]

VI. FOAMS: INTERNAL PRESSURE, EQUATION OF STATE, AND COMPRESSIBILITY

Up to this point, we have emphasized the common structural and other properties of concentrated emulsions and foams. However, because of their gaseous dispersed phase, foams are compressible and, just as gases themselves, can be characterized by an equation of state that relates their volume, external pressure, and temperature.

A. Dry-Foam Limit ($\phi = 1$)

For a polydisperse dry foam, one can define an average *internal pressure* \bar{p}_i that is given by

$$\bar{p}_i = \frac{\sum p_i v_i}{\sum v_i} = \frac{\sum p_i v_i}{V} \quad (55)$$

where p_i and v_i are the pressure and volume of bubble i , respectively, and V is the total foam volume. Derjaguin (70) has shown that

$$\bar{p}_i = P + \frac{2\sigma S_1}{3V} \quad (\phi = 1) \quad (56)$$

where P is the external pressure and S_1/V is the specific surface area of the foam. Assuming ideality of the gas phase, this leads to the *equation of state*

$$\left(P + \frac{2\sigma S_1}{3V}\right)V = n\mathfrak{R}T \quad (\phi = 1) \quad (57)$$

where n is the number of moles of gas in the foam. The same results were later obtained by Ross (71).

Morrison and Ross (72) have indicated that although Eqs. (56) and (57) are undoubtedly correct for monodisperse foams, a rigorous proof of their validity for *polydisperse* systems was lacking. Such proof has since been provided by Hollinger (73), Crowley (74), and Crowley and Hall (75).

Derjaguin (70) further showed that the compression modulus K is given by

$$K \equiv -V \frac{dP}{dV} = \frac{P + 2\bar{p}_i}{3} = P + \frac{4\sigma S_1}{9V} \quad (\phi = 1) \quad (58)$$

which compares to $K=P$ for a simple ideal gas.

The specific surface area in Eqs. (56)–(58) may be replaced by

$$\frac{S_1}{V} = \frac{S_1 S_0}{S_0 V} = \frac{3}{R_{32}} \frac{S_1}{S_0} \quad (59)$$

where, as earlier, R_{32} is the Sauter mean bubble radius and $S_1/S_0 \approx 1.083$ is the increase in surface area associated with the transition from spherical to polyhedral bubbles at equal volume.

B. Foams with Finite Liquid Content ($\phi < 1$)

We have shown (29) that, for this general case, Eqs. (56)–(58) are to be modified as follows:

$$\bar{p}_i = P + \frac{1-\phi}{\phi} \Pi + \frac{2\sigma S}{3V_1} \quad (60)$$

$$\left(P + \frac{1-\phi}{\phi} \Pi + \frac{2\sigma S}{3V_1}\right)\phi V = n\mathfrak{R}T \quad (61)$$

$$K = \frac{1}{\phi} \left[P + \frac{1-\phi}{3\phi} \Pi + (1-\phi)^2 \frac{d\Pi}{d\phi} + \frac{4\sigma S}{9V_1} \right] \quad (62)$$

where Π is the osmotic pressure, V_1 is the volume of the dispersed gas phase, and V is the total foam volume ($V_1 = \phi V$). For $\phi = 1$, Eqs. (56)–(58) are recovered.

Equations (60)–(62) may be written in the form

$$\bar{p}_i - P = \frac{\sigma}{R_{32}} \left(\frac{1-\phi}{\phi} \tilde{\Pi} + 2 \frac{S}{S_0} \right) \quad (63)$$

$$\left[P + \frac{\sigma}{R_{32}} \left(\frac{1-\phi}{\phi} \tilde{\Pi} + 2 \frac{S}{S_0} \right) \right] \phi V = nRT \quad (64)$$

$$K = \frac{1}{\phi} \left[P + \frac{\sigma}{R_{32}} \left(\frac{1-\phi}{3\phi} \tilde{\Pi} + (1-\phi)^2 \frac{d\tilde{\Pi}}{d\phi} + \frac{4}{3} \frac{S}{S_0} \right) \right] \quad (65)$$

where $\tilde{\Pi}$ is the reduced osmotic pressure. The terms within the parentheses depend on ϕ only and can be evaluated from the above-presented data. It may be shown (29) that the “osmotic” terms, although significant, provide only a rather small correction ($< 6\%$) to the dominant “Derjaguin terms” in S/S_0 . Of perhaps trivial but greater significance is the correction for the volume fraction outside the brackets of Eqs (61), (62), (64), and (65).

VII. MECHANICAL AND RHEOLOGICAL PROPERTIES

It has long been realized that the crowding of deformable drops and bubbles in concentrated emulsions and foams gives rise to interesting mechanical and rheological properties, not shown by the separate constituent fluid phases. When subjected quasistatically to a small stress, these systems respond as purely elastic solids, characterized by a static elastic modulus, G . Under dynamic conditions, the modulus has a real, elastic component (the storage modulus, G') and a complex, viscous component (the loss modulus, G''). Once a critical or yield stress is exceeded, the systems flow and behave as viscoelastic fluids, whose effective viscosity decreases from infinity (at the yield stress) with increasing shear rate. Thus, in rheological terms, they are *plastic* fluids with viscoelastic *solid* behavior below the yield stress and viscoelastic *fluid* behavior above the yield stress.

A number of early experimental studies have provided qualitative evidence for some or all of these behavioral aspects (e.g., Refs. 4 and 76–82), but the techniques employed were usually crude and/or the systems were poorly characterized, if at all. This makes it impossible to use these early experimental data to draw conclusions as to the quantitative relationships between the rheological properties, on the one hand, and important

system variables, such as volume fraction, interfacial tension, mean drop size (and size distribution), fluid viscosities, shear rate, and so forth, on the other hand. In the last decade or so, interest in this area has intensified and much progress has been and is being made along several fronts: theoretical modeling, computer simulation, and careful experimentation. For other recent, although by now somewhat outdated, reviews, see Refs. 83–86.

A. Theoretical Modeling and Computer Simulation

In view of the exceedingly complex structure of 3D systems—even when monodisperse—initial efforts were confined almost exclusively to their 2D analogs. Although unrealistic in some ways, these models provide important kinematic insights and their behavior may be extrapolated, with caution and limitations, to real systems. At first, for the sake of mathematical tractability, the complexity was reduced even further by considering perfectly ordered, *monodisperse* 2D systems. Gradually, the degree of complexity has been increased by allowing disorder. It is only very recently that some intrepid investigators have begun to tackle the 3D problem in earnest.

1. Elastic and Yield Properties: Shear Modulus and Yield Stress

Two-Dimensional Systems. For the perfectly ordered case, the unstrained equilibrium structure has been discussed earlier. The (cylindrical) drops are arranged on a perfectly ordered hexagonal lattice, decorated at its vertices with Plateau borders, whose wall curvatures are determined by the drop size and volume fraction according to Eq. (11). The system can be thought to be confined between two parallel plates, with rows of drops being forced to align with the plates. As one of the plates is now moved within its own plane to induce shear, all drops respond by being deformed identically. In the process, the surface area increases. With the assumption of constant interfacial tension, this results in a force (stress) versus deformation (strain) behavior that has been analyzed in detail, using straightforward geometrical arguments, by Princen (87) for any value of $\phi \geq \phi_0$. The simplest dry-foam case of $\phi = 1$ has been considered independently by Prud'homme (88).

The sequence of events in the dry-foam limit is illustrated in Fig. 23 for a single unit cell (i.e., the parallelogram formed by the centers of four adjacent drops). As the cell is strained at constant volume, the angle between the films must remain at 120° , which causes the central film to shorten until its length shrinks to zero. At that point, four films meet in a line. The resulting instability resolves itself by a rapid so-called T1 rearrangement or “neighbor switching.” In the process, new film is generated from the center to restore the original, unstrained configuration. A different, perhaps clearer, view of the system as it moves through such a cycle is shown in

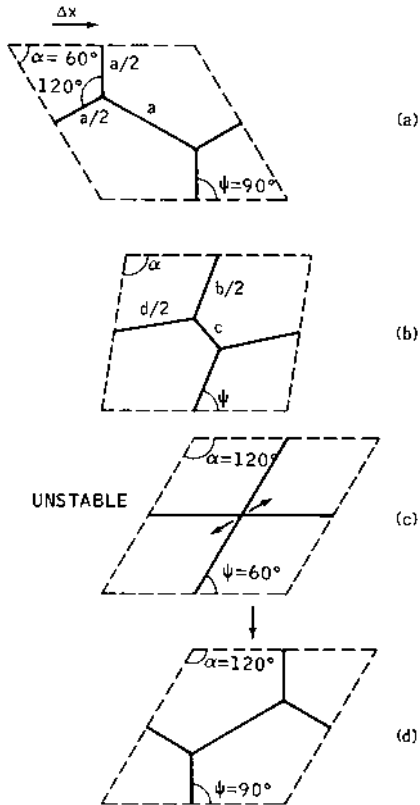


Figure 23 Shear deformation of unit cell of perfectly ordered 2D system in dry-foam limit ($\phi = 1$); the transition from (c) to (d) is rapid and is often referred to as a T1 rearrangement or neighbor switching. (From Ref. 87, with permission from Academic Press.)

Fig. 24. At any stage, the stress per unit cell is given by the horizontal component of the tension of the originally vertical films; that is,

$$F = 2\sigma \cos \psi \quad (66)$$

where ψ is the angle between these films and the horizontal shear direction. The resulting stress-strain curve per unit cell is given by curve 8 in Fig. 25, where \tilde{F} is the dimensionless stress per unit cell:

$$\tilde{F} = \frac{F}{2\sigma} = \cos \psi \quad (67)$$

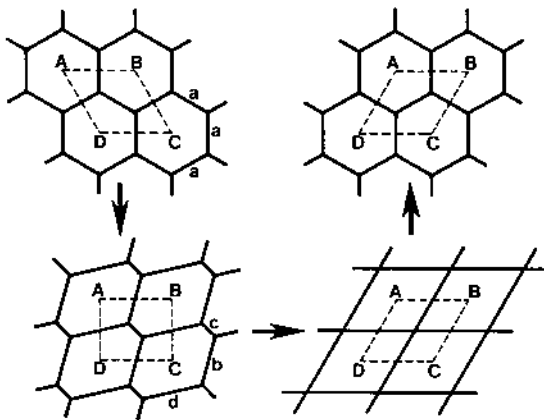


Figure 24 Alternative view of shear strain cycle. (From Ref. 87, with permission from Academic Press.)

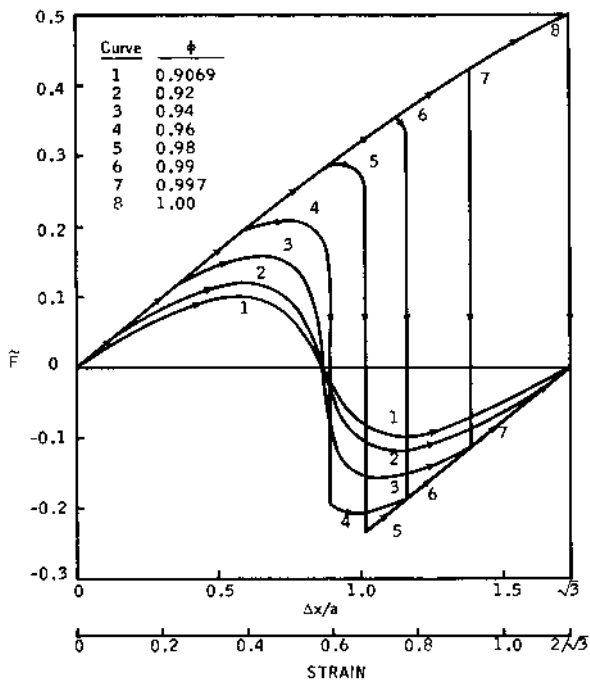


Figure 25 Shear stress per unit cell versus shear strain for perfectly ordered 2D system at different volume fractions. (From Ref. 87, with permission from Academic Press.)

Khan and Armstrong (45,89,90), using a slightly different analysis, arrived at the following simple analytical result for curve 8:

$$\tilde{F} = \frac{\gamma}{(\gamma^2 + 4)^{1/2}} \quad (68)$$

where γ is the imposed strain, which varies from zero to $2/\sqrt{3}$ at the point of instability. The cycle then repeats itself.

When $\phi < 1$, the situation is considerably more complicated (Fig. 26). As long as the two Plateau borders within the unit cell remain separated (Mode I), the stress per unit cell is unaffected. However, beyond a given strain, which depends on ϕ , the Plateau borders merge to form a single, four-sided border. In this Mode II regime, the films no longer meet at 120° , and the stress-strain curve deviates from that for the dry-foam limit.

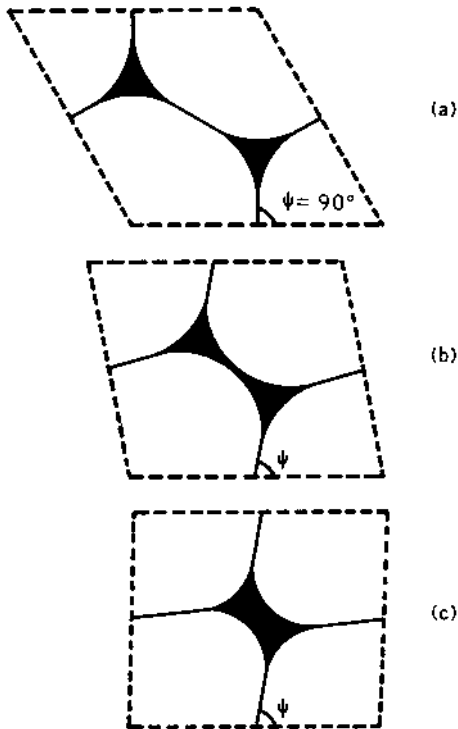


Figure 26 Increasing strain for systems with $0.9069 < \phi < 1$. Between (a) and (b), the system is in Mode I; between (b) and (c), the system is in Mode II. (From Ref. 87, with permission from Academic Press.)

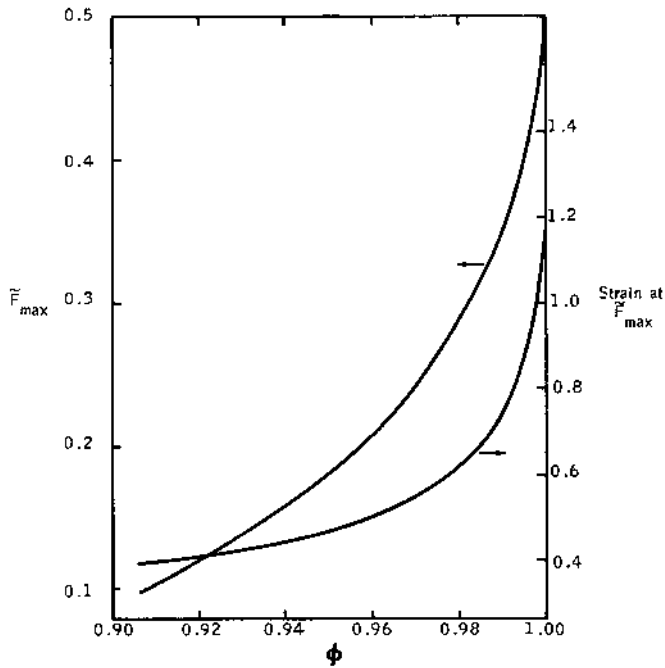


Figure 27 Static yield stress per unit cell and yield strain as a function of volume fraction for a perfectly ordered 2D system. (From Ref. 87, with permission from Academic Press.)

It passes through a (lower) maximum and ultimately reverses sign, either continuously or via a T1 rearrangement (87). The resulting curves are collected in Fig. 25. In each case, the maximum \tilde{F}_{\max} corresponds to the static *yield stress* per unit cell. It is plotted in Fig. 27 as a function of ϕ , together with the corresponding yield strain. Realizing that there are $1/a\sqrt{3}$ unit cells per unit of length in the shear direction and that a may be expressed in terms of the more practical drop radius R and volume fraction ϕ , one finds for the stress(τ)–strain(γ) relationship

$$\tau = 1.050 \frac{\sigma}{R} \phi^{1/2} \tilde{F}(\gamma, \phi) \quad (69)$$

whereas the *yield stress*, τ_0 , is given by

$$\tau_0 = 1.050 \frac{\sigma}{R} \phi^{1/2} \tilde{F}_{\max}(\phi) \quad (70)$$

where $\tilde{F}_{\max}(\phi)$ may be read from Fig. 27. It is expected to start deviating from zero when adjacent layers of close-packed drops or bubbles can freely slide past each other (i.e., at $\phi = \pi/4 = 0.7854$).

The small-strain, static *shear modulus*, G , is defined as

$$G \equiv \left(\frac{d\tau}{d\gamma} \right)_{\gamma=0} \quad (71)$$

and can be obtained from Eqs. (69) and (68):

$$G = 1.050 \frac{\sigma}{R} \phi^{1/2} \left(\frac{d\tilde{F}}{d\gamma} \right)_{\gamma=0} = 0.525 \frac{\sigma}{R} \phi^{1/2} \quad (\phi > \phi_0) \quad (72)$$

The model predicts zero shear modulus for $\phi < \phi_0$.

Both the yield stress and the shear modulus scale with σ/R , but, although the yield stress increases strongly with volume fraction, the shear modulus is affected only very weakly through $\phi^{1/2}$. In the dry limit of $\phi = 1$, both reach identical limiting values of

$$\tau_0 = G = 0.525 \frac{\sigma}{R} \quad (\phi = 1) \quad (73)$$

The analysis may be extended to systems in which the film thickness, h , or the contact angle, θ , between the films and the Plateau border walls are finite (87). The effect of a finite film thickness is to increase the effective volume fraction [cf. Eq. (1)], which raises the yield stress and shear modulus in a predictable fashion. The effect of a finite contact angle on the shear modulus is to simply reduce it by a factor of $\cos \theta$. The effect on the yield stress is more complex. In most but not all cases, the yield stress is increased. Furthermore, a finite contact angle can give rise to interesting new instability modes and to hysteretic behavior. The reader is referred to Ref. 87 for further details.

Subsequently, Khan and Armstrong (89,90) and Kraynik and Hansen (91) considered the effect of the orientation of the unit cell, relative to the shear direction, for the dry-foam case. They found that the shear modulus is unaffected, but that the yield stress is sensitive to the orientation. In addition, they considered planar extension as well as shear.

The sudden jump of the shear modulus from zero to a finite value at ϕ_0 and its subsequent weak sensitivity to ϕ for $\phi > \phi_0$ are rather peculiar and appear to be associated with the perfect order of the model. The pure cyclical character of the stress-strain curves is—by itself—a symptom of

“perfection pathology.” Real systems do not exhibit these particular features, because they are invariably disordered, which causes T1 rearrangements to occur even at very small strains, as well as randomly throughout the system, rather than simultaneously at all vertices.

The shear modulus of polydisperse hexagonal systems of the type depicted in Fig. 8b, is still given by Eq. (72) when R is replaced by $R_{\text{av}} = (\sum R_i^2/n)^{1/2}$, a characteristic drop radius that is based on the average drop area (46). However, as expected, the “elastic limit” (i.e., the stress and strain where the first T1 rearrangement occurs) is reduced relative to that of the monodisperse case of the same volume fraction.

The elastic and yield properties of 2D systems with the most general type of disorder (cf. Fig. 7) have been simulated by Hutzler et al. (92) for both dry and wet systems. Indeed, as the number of polydisperse drops in the simulation is increased, the jumps in stress associated with individual or cooperative T1 rearrangements become less and less noticeable. Instead, the stress increases smoothly with increasing strain until it reaches a plateau that may be identified with the yield stress. The yield stress was found to increase sharply with increasing volume fraction, very much as in the monodisperse case. Furthermore, the shear modulus for the dry system ($\phi = 1$) was essentially identical to that for the monodisperse case, as given by Eq. (73) with R_{av} , as defined earlier, replacing R . Its dependence on ϕ was very different from that in Eq. (72), however. When expressed in our terms, their results for $1 > \phi > 0.88$ could be fitted to

$$\frac{G}{\sigma/R_{\text{av}}} = 0.51 - 21(1 - \phi)^2 \quad (74)$$

Assuming that this relationship continues to hold for $\phi < 0.88$ (where their simulations ran into difficulties because of the large number of T1 processes the program had to deal with), the authors (92) concluded that G reaches zero at $\phi = \phi_0 \approx 0.84$. As mentioned earlier, this “rigidity-loss transition” can be identified as the random close packing of hard disks. The drop in G with decreasing ϕ could further be correlated with the average number of sides of the Plateau borders, which gradually increased from three close to $\phi = 1$ to about four at $\phi = 0.84$. Although these simulations involved a rather small number of drops and leave some questions unanswered, they do indicate a type of elastic behavior that—as we will see later—much more closely reflects that of real systems. Clearly, disorder plays a critical role.

Three-Dimensional Systems. The first expression for the shear modulus of random dry foams (and emulsions) was derived by Derjaguin (93). It is based on the assumption that the foam is a collection of randomly

oriented films of constant tension 2σ and negligible thickness and that each film responds affinely to the applied shear strain, as would an imaginary surface element in a continuum. Evaluating the contribution to the shear stress of a film of given orientation and averaging over all orientations then leads to

$$G = \frac{4}{15} \sigma \frac{S_1}{V} \quad (\phi \approx 1) \quad (75)$$

where S_1/V is the surface area per unit volume. Because $S_1/V \approx 1.083 S_0/V = 3.25/R_{32}$, this may be written as

$$G \approx \frac{13}{15} \frac{\sigma}{R_{32}} \approx 0.87 \frac{\sigma}{R_{32}} \quad (\phi \approx 1) \quad (76)$$

Much later, Stamenović and Wilson (94) rediscovered Eq. (75), using similar arguments but pointing out at the same time that it probably represents an overestimate. Indeed, using 2D arguments, Princen and Kiss (95) concluded that the affine motion of the individual films violates Plateau's laws and leads to an overestimate of G by a factor of 2, at least in 2D. (Kraynik, in a private communication, pointed out an internal inconsistency in Ref. 95 and concluded that G is overestimated by a factor of only 3/2). Furthermore, Derjaguin's model does not allow for T1 rearrangements; it does not predict a yield stress nor does it have anything to say about the effect of ϕ in "wet" systems. On the other hand, the model correctly predicts that G scales with σ/R .

Stamenović (96) analyzed the deformation of an idealized single foam vertex, where four Plateau borders meet and concluded that

$$G = \frac{1}{6} \sigma \frac{S_1}{V} \approx 0.54 \frac{\sigma}{R_{32}} \quad (\phi \approx 1) \quad (77)$$

As pointed out by Reinelt and Kraynik (56), however, the idealized vertex does not adequately represent an equilibrium structure. Similar reservations apply to the work of Budiansky and Kimmel (97), who considered the behavior of an isolated foam cell in the form of a regular pentagonal dodecahedron and obtained a shear modulus between the two above values.

Using Brakke's Surface Evolver (49), Reinelt and co-workers (56,68,98–102) have explored in detail the elastic response of monodisperse, perfectly ordered structures, both "dry" and "wet," to extensional and shear strain. Structures considered included the rhombic dodecahedron, the regular ("planar") tetrakaidecahedron, the Kelvin cell, and the Weaire–Phelan

Table 1 Shear Moduli of Dry Systems

	$G_1/\sigma V^{-1/3}$	$G_2/\sigma V^{-1/3}$	$G_{av}/\sigma V^{-1/3}$	$G_{av}/\sigma R^{-1}$
Regular tetrakaidecahedron	0.5525	0.9696	0.8028	0.4980
Kelvin	0.5706	0.9646	0.8070	0.5006
Weaire–Phelan	0.8902	0.8538	0.8684	0.5387
Random (monodisperse)			0.78 ± 0.08	0.48 ± 0.05

structure. Some degree of disorder was introduced by considering bidisperse Weaire–Phelan systems (103), in which the relative volumes of the dodecahedra and tetrakaidecahedra were varied, as well as random, although monodisperse, systems (68). As in the 2D case, the stress–strain behavior depends on the cell orientation relative to the strain direction. Because of the multitude of edges and faces of each cell, a variety of T1 transitions may occur at increasing strain, leading to very complex behavior. Some of their results for the shear moduli of dry systems ($\phi = 1$) are listed in Table 1.

The ordered structures are all anisotropic, have cubic symmetry, and can be characterized by two shear moduli, G_1 and G_2 . To simulate orientational disorder, the authors introduced an “effective isotropic shear modulus,” $G_{av} = (2/5)G_1 + (3/5)G_2$, which is obtained by averaging over all orientations. The first three columns of Table 1 give the moduli in units of $\sigma V^{-1/3}$, where V is the cell volume; the last column is given in units of σ/R , where $R = (3V/4\pi)^{1/3}$. The orientation-averaged results are surprisingly close to the 2D prediction of $G/\sigma R^{-1} = 0.525$ [cf. Eq. (73)], Stamenović’s prediction of $G/\sigma R^{-1} = 0.54$ [cf. Eq. (77)], and the extrapolated experimental result of Princen and Kiss (95) for polydisperse emulsions, which indicated that $G/\sigma R_{32}^{-1} = 0.509$ (see Sect. VII.B.3). The small influence of polydispersity is also suggested by the finding that G_{av} varies less than 0.5% when the volume ratio of the two types of cells in bidisperse Weaire–Phelan structures is varied between 0.039 and 2.392 (103).

Simulations of this type can pinpoint an “elastic limit” where the first (or subsequent) T1 transition(s) take(s) place. It depends extremely strongly on orientation, as does the “dynamic yield stress” (i.e., the stress integrated over a complete strain cycle). The relevance to the yield stress of real disordered systems is therefore quite limited (100). As in 2D simulations, simulations on more highly disordered systems will undoubtedly bring increased insight.

Simulations on “wet” rhombic dodecahedra and Kelvin cells have been carried out by Kraynik and colleagues (68,102). The effective isotropic shear moduli were found to depend slightly on the volume fraction but did not show the linear dependence on $\phi - \phi_0$ found experimentally for

disordered systems (95). Again, simulations on highly disordered wet systems should improve our understanding.

Buzza and Cates (104) also addressed the question of whether disorder or the increased dimensionality from two to three dimensions is responsible for the observed experimental behavior of the shear modulus. In particular, they explored the lack of the sudden jump in G from zero to a finite value at $\phi = \phi_0$ that is predicted by the perfectly ordered 2D model. We have seen earlier that disorder appears to remove that abrupt jump in two dimensions (92). For drops on a simple cubic lattice, Buzza and Cates analyzed the drop deformation in uniaxial strain close to $\phi = \phi_0$, first using the model of “truncated spheres.” (For reasons given earlier, we believe this to be a very poor model.) They showed that this model did not eliminate the discontinuous jump in G . An exact model, based on a theory by Morse and Witten (105) for weakly deformed drops, led to $G \propto 1/\ln(\phi - \phi_0)$, which gets rid of the discontinuity but still shows an unrealistically sharp rise at $\phi = \phi_0$ and is qualitatively very different from the experimentally observed linear dependence of G on $\phi = \phi_0$. Similar conclusions were reached by Lacasse and co-workers (51,106). A simulation of a disordered 3D model (106) indicated that the droplet coordination number increased from 6 at ϕ_0 to 10 at $\phi = 0.84$, qualitatively similar to what is seen in disordered 2D systems (92). Combined with a suitable (anharmonic) interdroplet force potential, the results of the simulation were in close agreement with experimental shear modulus and osmotic pressure data. Therefore, it appears again that disorder is responsible for many of the features of real systems.

2. Shear Viscosity

Compared to the quasistatic elastic and yield behaviors of concentrated emulsions and foams, the rate-dependent viscous properties are even more complex and relatively unexplored. Formally, the shear stress, τ , may be expressed as a function of the shear rate, $\dot{\gamma}$, as

$$\tau(\dot{\gamma}) = \tau_0 + \tau_s(\dot{\gamma}) \quad (78)$$

where τ_0 is the (elastic) yield stress and $\tau_s(\dot{\gamma})$ is the contribution from any rate-dependent dissipative processes; or, in terms of the effective shear viscosity, μ_e ,

$$\mu_e \equiv \frac{\tau(\dot{\gamma})}{\dot{\gamma}} = \frac{\tau_0}{\dot{\gamma}} + \frac{\tau_s(\dot{\gamma})}{\dot{\gamma}} \quad (79)$$

The first term is, to a large extent, responsible for the shear-thinning behavior of these systems. As is clear from the previous discussion, τ_0 is determined primarily by σ , R and ϕ , whereas the size distribution may play a secondary

role. The dynamic stress, τ_s , is expected to depend on these and other variables (e.g., the shear rate, the viscosities of the continuous and dispersed phases, and surface-rheological parameters). So far, the predictive quality of theoretical and modeling efforts has been very restricted because of the complexity of the problem.

Buzza et al. (107) have presented a qualitative discussion of the various dissipative mechanisms that may be involved in the small-strain linear response to oscillatory shear. These include viscous flow in the films, Plateau borders, and dispersed-phase droplets (in the case of emulsions), the intrinsic viscosity of the surfactant monolayers, and diffusion resistance. Marangoni-type and “marginal regeneration” mechanisms were considered for surfactant transport. They predict that the zero-shear viscosity is usually dominated by the intrinsic dilatational viscosity of the surfactant monolayers. As in most other studies, the discussion is limited to small-strain oscillations, and the rapid events associated with T1 processes in steady shear are not considered, even though these may be extremely important.

It is now generally recognized that surfactants are indeed crucial, not only in conferring (meta)stability to the emulsion or foam but also in controlling the rate-dependent rheology of the film surfaces and that of the system as a whole. Several early, spatially periodic 2D models neglected this aspect and made other simplifying assumptions. Khan and Armstrong (45,89,90) and Kraynik and Hansen (108) assumed that all of the continuous phase resides in the films (i.e., there were no Plateau borders) and that there is no exchange of fluid *between* the films. The film surfaces were assumed to be completely mobile (no surfactant!). When such a system is strained globally, the uniform films respond with simple planar extension (or compression) at constant volume. This mechanism predicts significant structural changes but leads to viscous terms in Eqs. (78) and (79) that are insignificant compared with the elastic terms up to extremely high shear rates that are unlikely to be encountered in practice. Experimentally, one finds a much more significant contribution (see Sect. VII.B.3).

A more complete 2D analysis of simple shear is that of Li et al. (109). It solves the detailed hydrodynamics in the drops, films, and Plateau borders for the case of equal viscosities of the continuous and dispersed phases. Again, large structural changes are predicted. However, surfactants (and surface tension gradients) are assumed to be absent, which severely limits the practical implications of the analysis. An interesting conclusion is that, under certain conditions, shear flow can stabilize concentrated emulsions, even in the total absence of surfactants.

An approach that is almost diametrically opposed to the earlier models of Khan and Armstrong, and Kraynik and Hansen, was advanced by Schwartz and Princen (110). In this model, the films are negligibly thin,

so that all of the continuous phase is contained in the Plateau borders and the surfactant turns the film surfaces immobile as a result of surface tension gradients. Hydrodynamic interaction between the films and the Plateau borders is considered to be crucial. This model, believed to be more realistic for common surfactant-stabilized emulsions and foams, draws on the work of Mysels et al. (111) on the dynamics of a planar, vertical soap film being pulled out of, or pushed into, a bulk solution via an intervening Plateau border. An important result of their analysis is commonly referred to as Frankel's law, which relates the film thickness, $2h_\infty$, to the pulling velocity, U , and may be written in the form

$$\frac{h_\infty}{r} = 0.643(3Ca^*)^{2/3} \quad (80)$$

where $Ca^* = \mu U/\sigma$ ($\ll 1$) is the film-level capillary number, μ and σ are the viscosity and surface tension of the liquid (the "continuous phase"), and r is the radius of curvature of the Plateau border where it meets the film and is given by capillary hydrostatics, $r = (\sigma/2\rho g)^{1/2}$, where ρ is the density of the liquid and g is the gravitational acceleration.

Frankel's law has its close analogs in a number of related problems (112–114) and has been verified experimentally (115,116) in the regime where the drawn-out film thickness, $2h_\infty$, is sufficiently large for disjoining-pressure effects to be negligible. Below some critical speed, the thickness of the drawn-out film equals the finite equilibrium thickness, $2h_{eq}$, which is set by a balance of the disjoining pressure, $\Pi_d(h)$, and the capillary pressure, σ/r , associated with the Plateau border. Thus, Frankel's law and the following analysis apply only as long as $1 \gg Ca^{*2/3} \gg h_{eq}/r$. It is expected to break down as the capillary number approaches zero. Disjoining pressure effects may, in principle, be included (e.g., Ref. 117) but at the expense of simplicity and generality of the model.

The interesting hydrodynamics and the associated viscous energy dissipation are confined to a transition region between the emerging, rigidly moving film and the macroscopic Plateau border. The lubrication version of the Stokes equation may be used in this region, as the relative slope of the interfaces remains small there.

It is reasonable to assume that the same basic process operates in moving emulsions and foams. Lucassen (118) has pointed out that for such systems to be stable to deformations such as shear, the dilatational modulus of the thin films must be much greater than that of the surfaces in the Plateau border. However, this is equivalent to the assumption of inextensible film surfaces that underlies Frankel's law. Therefore, it may well be that, by implication, emulsions and foams that are stable to shear (and we

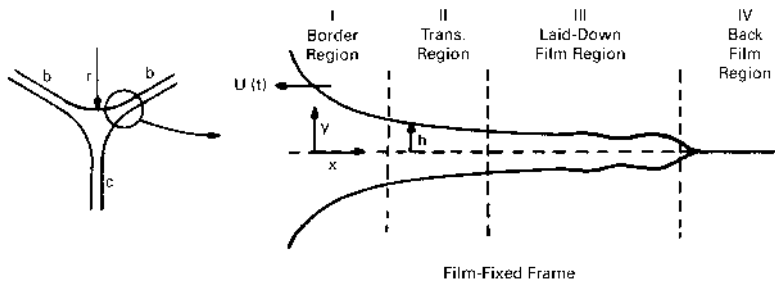


Figure 28 Film being pulled out of a Plateau border with velocity $U(t)$; all viscous dissipation occurs in the transition region (II). (From Ref. 110, with permission from Academic Press.)

are interested in such systems only) have the appropriate surface rheology for Frankel's law to apply. Of course, in emulsions and foams, each Plateau border of radius r (set by drop size and volume fraction) is now shared by three films. At any given moment, one or two of the films will be drawn out of the border while the other(s) is (are) pushed into it, at respective quasi-steady velocities $U(t)$ that are dictated by the macroscopic motion of the system (Fig. 28). Using a perfectly ordered 2D system, Schwartz and Princen (110) considered a periodic uniaxial, extensional strain motion of small frequency and amplitude, so that inertial effects are negligible and complications due to the merger of adjacent Plateau borders and associated rapid T1 processes are avoided. They proceeded by calculating the instantaneous rate of energy dissipation in the transition region of each of the three films associated with a Plateau border and integrated the results over a complete cycle. When the effective strain rate is related to the frequency of the imposed motion, the result can be expressed as an effective viscosity that is given by*

$$\mu_e = 5.3\mu Ca^{-1/3} \quad (81)$$

where the macroscopic capillary number $Ca \equiv \mu a \dot{\gamma} / \sigma$, a is the length of the hexagon that circumscribes a drop or bubble, and μ is the viscosity of the continuous phase. Because of the small amplitude of the imposed motion,

*In the original article (110), the numerical coefficient was given as 6.7. This and a few other minor numerical errors were pointed out by Reinelt and Kraynik (119, and private communication).

the result does not depend on the volume fraction. It was further argued that in the case of emulsions, the effect of the dispersed-phase viscosity, μ_d , is relatively insignificant. Reinelt and Kraynik (120) later estimated that this is a good approximation as long as

$$\frac{\mu_d}{\mu} \ll \text{Ca}^{-1/3} \quad (82)$$

Apart from a change in the numerical coefficient, Eq. (81) is expected to apply also to a periodic, small-amplitude *shearing* motion. However, in *steady shear*, rapid film motions associated with the T1 processes, whose effect has so far not been analyzed, periodically interrupt the above process. Further, as the strain at the instability depends on the volume fraction (Fig. 27), the viscous term may become ϕ dependent. Provided that the effect of the T1 jumps may be neglected or the associated viscous contribution also scales with $\mu\text{Ca}^{-1/3}$, this model would then predict for the shear viscosity,

$$\mu_e = \frac{\tau_0}{\dot{\gamma}} + C(\phi)\mu\text{Ca}^{-1/3} = \frac{\tau_0}{\dot{\gamma}} + C'(\phi)\frac{\mu^{2/3}\sigma^{1/3}}{R^{1/3}}\dot{\gamma}^{-1/3} \quad (83)$$

or, for the shear *stress*,

$$\tau = \tau_0 + C(\phi)\frac{\sigma}{a}\text{Ca}^{2/3} = \tau_0 + C'(\phi)\frac{\mu^{2/3}\sigma^{1/3}}{R^{1/3}}\dot{\gamma}^{2/3} \quad (84)$$

where $C(\phi)$ and $C'(\phi)$ are of order unity and the yield stress τ_0 is given by Eq. (70). Equations (83) and (84) describe a particular type of ‘‘Herschel–Bulkley’’ behavior, characterized in general by $\tau = \tau_0 + K\dot{\gamma}^n$ and $\mu_e = \tau_0/\dot{\gamma} + K\dot{\gamma}^{n-1}$. The special case of $n=1$ is referred to as ‘‘Bingham plastic’’ behavior. Occasionally, foams and concentrated emulsions are claimed to behave as Bingham fluids. As we shall see, this is not so. (In fact, it is extremely unlikely that *any* fluid, when examined carefully, can be described as such.)

Reinelt and Kraynik (119) improved on the above model by including structural changes that result from the fact that the film tensions deviate from the equilibrium value of 2σ as they are being pulled out of or pushed into the Plateau border. These changes are of order $(\text{Ca}^*)^{2/3}$, as already pointed out by Mysels et al. (111). As the values and signs of Ca^* at any instant are different for the three films emanating from a Plateau border, their tensions are generally unequal and the angles between them deviate from 120° , and the Plateau border radius, r , is also affected. However, these refinements do not alter the qualitative conclusion of the original model, as embodied in Eq. (81), for either planar-extensional or shear deformations.

Applying this approach to uniform dilatation of a foam, Reinelt and Kraynik (119) also derived an expression for the dilatational viscosity, which again scales with $\mu\text{Ca}^{-1/3}$. Using a different surface-rheological description, Edwards and co-workers (121–123) arrived at alternative expressions for the dilatational viscosity of wet and dry foams.

In yet another extension, Reinelt and Kraynik (120) applied the approach to *steady shearing* and *planar-extensional* flow of perfectly ordered 2D systems for $0.9069 < \phi < 0.9466$. This is the range of “very wet” systems, for which the shear stress varies continuously with strain over a complete strain cycle (cf. Fig. 25), so that rapid film events associated with T1 processes are avoided. They also investigated the effect of orientation, and structural effects due to changes in film tension were again included. As earlier, the effective viscosity was found to be proportional to $\mu\text{Ca}^{-1/3}$. Interestingly, the model indicates that the effective viscosity increases with increasing volume fraction, which parallels practical experience.

Okuzuno and Kawasaki (124) simulated the shear rheology of dry, random 2D systems, using their “vertex model” in which the films are uncurved and do not generally meet at 120° angles. Although Plateau’s condition is therefore violated, the model offers the advantage of being computationally more efficient than other, more realistic models. By solving the “equations of motion” for all the vertices, while taking account of T1 rearrangements and using the energy-dissipation approach of Schwartz and Princen (110), these authors tentatively concluded that the system behaves like a Bingham plastic fluid. However, because the number of simulations was quite limited, they did not rule out Herschel–Bulkley behavior with $n \neq 1$ (see above discussion). In a later study, the same investigators (125) observed violent flows like that of an avalanche in their simulations in the large strain regime at small shear rate. Similar avalanchelike flows are observed in simulations by Jiang et al. (126).

This review is not exhaustive by any means. Other studies have been and are being published regularly, as the topic continues to enjoy considerable interest. It appears, however, that theoretical analyses and computer simulations can only go so far. There is a need for careful experimental work in order to establish the *actual* behavior of real systems. As has been the case in the past, further progress will be optimal when the two approaches go hand in hand.

B. Experimental Approaches and Results

The rheological parameters of primary scientific and practical concern are the static and dynamic shear modulus, the yield stress, and the shear-rate-dependent viscosity. The aim is to understand and predict how these

depend on the system parameters. In order to accomplish this with any hope of success, there are two areas that need to be emphasized. First, the systems studied must be characterized as accurately as possible in terms of the volume fraction of the dispersed phase, the mean drop size and drop size distribution, the interfacial tension, and the two bulk-phase viscosities. Second, the rheological evaluation must be carried out as reliably as possible.

1. System Characterization

The bulk phases are generally Newtonian and their *viscosities* can be measured with great accuracy with any standard method available.

The *nominal volume fraction* of the dispersed phase can be obtained very accurately from the relative volumes (or weights) of the phases used in the preparation of a highly concentrated emulsion (69). A series of emulsions, differing only in volume fraction, may be conveniently prepared by dilution of a mother emulsion with varying known amounts of the continuous phase (69). Alternatively, if the phases differ greatly in volatility, the volume fraction may be obtained, albeit destructively, from the weight loss associated with evaporation of the more volatile phase, usually water (127). Another destructive method is to destroy the emulsion by high-speed centrifugation in a precision glass tube, followed by accurate measurement of the relative heights of the separated liquid columns (24). To arrive at the *effective volume fraction*, the nominal volume fraction may need to be corrected for a finite film thickness according to Eq. (1). Because all rheological parameters depend more or less strongly on the volume fraction, it is important that the vertical gradient in volume fraction due to gravity be kept to a minimum, if reliable rheological evaluations are to be expected. The gradient in volume fraction may be predicted quantitatively (67). Because the drop size and the density difference between the phases are generally much larger in foams than in emulsions, the gradient in ϕ is usually much more pronounced in the former than in the latter. The rheologies of both types of system being governed by identical laws, it is preferable—for this and many other reasons (see next paragraph)—to use *emulsions*, rather than foams, to learn about *foam* rheology.

The *mean drop size* and *drop size distribution* can be measured to within a few percent accuracy with a number of techniques, such as the “Coulter Counter” (69,95,128) and dynamic light scattering. The Coulter Counter is eminently suitable for oil-in-water emulsions but has a lower practical limit of about 1 μm . Various light-scattering techniques are equally suitable for oil-in-water and water-in-oil (w/o) emulsions and afford a larger dynamic range. In either case, the concentrated emulsion must be diluted with the continuous phase to a level where coincidence counting or multiple

scattering, respectively, is avoided. One popular method that should perhaps be avoided is optical microscopy, which is not only tedious but also relatively inaccurate when applied to polydisperse systems because of depth-of-focus limitations and wall effects. At any rate, a practical lower limit for accurate, quantitative optical microscopy is well in excess of $1\ \mu\text{m}$. Whatever method is used, it is desirable that complete size distributions be reported. At the very least, when only a mean drop size is reported, the *type* of mean should be specified. Finally, it appears that size determinations are much easier to obtain in emulsions than in foams. Moreover, although it is easy to prepare emulsions whose drop size distribution changes imperceptibly over a period of months, the bubble size distribution in foams changes very rapidly as a result of Ostwald ripening. It is, therefore, almost impossible to have accurate knowledge of the bubble size distribution at the moment a rheological measurement is being made. These are yet additional reasons for using emulsions in order to investigate foams.

The *interfacial tension* may be determined to within about 1% accuracy with the spinning drop method (129,130). It is an absolute and static method that requires only small samples and, in contrast to most other methods, does not depend on the wettability of a probe, such as a ring or Wilhelmy plate. The stabilizing surfactant is commonly used at concentrations in the bulk continuous phase that are far above the critical micelle concentration (cmc). This ensures that the concentration remains above the cmc after adsorption onto the vastly extended interface has taken place, which is clearly needed to maintain emulsion stability. It is tempting, therefore, to assume that the interfacial tension in the finished emulsion equals that between the unemulsified bulk phases and that it remains constant when a “mother emulsion” is diluted with continuous phase in order to create a series of emulsions in which only ϕ is varied (69). This may be a reasonable assumption when a pure surfactant is used, but there is evidence that this may not be so when impure commercial surfactants are employed (95,128).

2. Rheological Evaluation

Most studies have used standard rheological techniques, such as rotational viscometers of various types and geometries, such as concentric-cylinder, cone-and-plate, and parallel-plate rheometers, each of which may be operated in various modes [constant stress, constant strain, steady shear, or dynamic (i.e., oscillatory) shear]. The relative advantages and/or limitations of these and other techniques may be found in any standard textbook on practical rheometry (e.g., Ref. 131). When applied to highly concentrated emulsions and foams—or suspensions in general, for that matter—these

techniques are fraught with many difficulties and pitfalls that are often overlooked, leading to results of questionable validity. Some of these difficulties are the following.

Wall-induced Instability. Princen (69) has reported that otherwise very stable oil-in-water emulsions showed extremely erratic behavior when sheared in a commercial concentric-cylinder viscometer with stainless-steel parts. The problem could be traced to the “coalescence” of the dispersed oil droplets with the steel walls and the formation of a thick oil layer. Apparently, the thin films of continuous phase separating the walls from the first layer of individual droplets were unstable and ruptured. Coating all relevant parts with a thin film of silica, which assured adequate film stability and complete wetting of the steel by the continuous phase, solved the problem (69). Later, an even more satisfactory solution consisted of replacing the steel inner and outer cylinders with glass parts, combined with other improvements in design (95,128,132). Some of the glass cylinders were highly polished; others were roughened and equipped with vertical grooves to eliminate or reduce wall slip (see below). Wall-induced instability may or may not be a problem, depending on the wall material, the emulsion (w/o or o/w), and surfactant type.

End and Edge Effects. In the analysis of raw data obtained with any type of rotational viscometer, it is assumed that the flow field is known and simple. For example, in the conventional concentric-cylinder viscometer, it is assumed that the fluid moves in concentric cylindrical layers that extend unchanged from the precise top to the precise bottom of the inner cylinder. This is true only when the cylinders are infinitely long. For cylinders of finite length, complications at the top are usually minor and can often be neglected. In the lower region of the viscometer, however, the flow is seriously disturbed. In addition, the bottom of the inner cylinder may contribute a substantial fraction of the total measured torque. This can lead to serious errors. Various suggestions have been made to deal with the problem (131), but their practical value is questionable. In addition to making other improvements, including the use of a *hollow* inner cylinder, Princen and Kiss (95,128,132) effectively isolated the bottom region by filling it with a layer of mercury. In that way, the sample of interest is strictly confined to the space between the cylinders. As long as its effective viscosity is much greater than that of mercury, flow between the cylinders is undisturbed and the torque on the bottom of the inner cylinder is negligible. The arrangement is shown schematically in [Fig. 29](#).

In the cone-and-plate viscometer, there are similar, although perhaps somewhat less severe, problems associated with the outer edge (131).

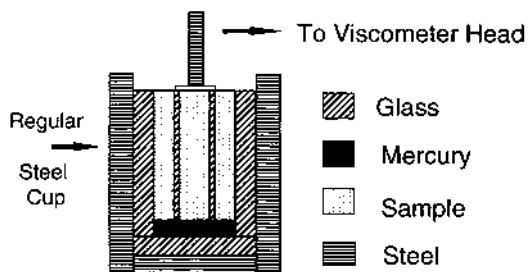


Figure 29 Modified concentric-cylinder viscometer with glass outer cylinder, hollow glass inner cylinder, and pool of mercury to confine the sample to the gap and thus to minimize the end effect.

Wall Slip. Along with wall-induced instability, the occurrence of slip between the sample and the viscometer walls is one of the most serious and prevalent, although often neglected, problems one encounters in assessing the rheology of dispersed systems, in general, and concentrated emulsions in particular. Because concentrated emulsions have a yield stress, wall slip—if present—can be readily demonstrated by painting a thin line of dye on top of the sample in a wide-gap rotating-cylinder viscometer (69). As long as the yield stress is not exceeded at the inner cylinder wall, the sample is not sheared at all but is seen to move around in the gap as an elastically strained solid! In this regime, shear is confined to the thin films of continuous phase separating the wall from the adjacent droplets. For a sufficiently smooth wall, it is possible to estimate the thickness of these films from the measured wall stress and angular velocity (69).

It is obvious that neglect of wall slip may lead to meaningless conclusions as to the system's rheology. There are two different approaches to dealing with this particular problem. First, one can try to eliminate slip by roughening the viscometer surfaces. Princen and Kiss (95) successfully used roughened and grooved glass cylinders to determine the static shear modulus of concentrated emulsions. This worked well in the low-stress, linear elastic regime, although, even here, some wall creep did occur (which could be readily corrected for). However, massive wall slip was noted to commence at shear stresses exceeding only about one-half of the bulk yield stress. Thus, even though the roughness was commensurate with the drop size and served the intended purpose, the arrangement would have been inadequate for determining the yield stress and shear viscosity. Therefore, the question remains how rough a surface must be to eliminate slip up to the maximum shear stress considered. As an extreme case, large radial vanes have been recommended, at least for yield stress

measurements (133). Although undoubtedly effective in preventing slip, the vanes do lead to some uncertainty in the strain field.

Many published rheological studies declare that wall slip was checked for and found to be absent. Unless solid evidence is provided, it behooves the reader to approach such assertions with a healthy dose of skepticism.

A second approach is to permit slip and to correct for it. This usually involves running the sample in two or more viscometer geometries (e.g., at different gap widths) (131,134,135). Doubts have been expressed as to the validity of this approach (136). At any rate, the procedure is rather tedious and may not be very accurate. In an alternative method, Princen and Kiss (128), using their improved design with polished glass cylinders, established empirically that the torque versus angular velocity data for concentrated emulsions may be linearized over most of the all-slip/no-flow regime. The stress at which the data deviated from this linear behavior was identified as the yield stress. Under the further, reasonable assumption that the linearized slip behavior persists above the yield stress, where flow commences, the angular velocity could be corrected for wall slip. Following standard rheological procedures for yield-stress fluids in a wide-gap concentric-cylinder viscometer, the dependence of the effective viscosity on shear rate could then be determined.

It is clear from the above discussion that extreme care must be exercised in the characterization and rheological evaluation of concentrated emulsions. Few, if any, commercial viscometers are designed to give reliable results for non-Newtonian fluids. Not only are modifications of the hardware often called for, but also the software of automated instruments is generally incapable of dealing with yield stress fluids, end effects, and wall slip. For example, to correct for end effects, it will not do to use a calibration or “instrument factor” for any but Newtonian fluids. Unfortunately, there are no shortcuts in this field!

3. Experimental Results

For reasons indicated earlier, accurate physical characterization and rheological evaluation of *foams* is extremely difficult. Indeed, although there is much published material on foams that is qualitatively consistent with what one would expect (and much that is not), we are not aware of any such studies that can stand close quantitative scrutiny. Therefore, we shall restrict ourselves to what has been learned from *highly concentrated emulsions*, whose rheology is, in any case, expected to be identical to that of foams in most respects. However, even in the emulsion area, the number of carefully executed studies is severely limited. Admittedly not without some prejudice, we shall concentrate on the systematic experimental work

by two groups that were active at different times at the Corporate Research Laboratory of Exxon Research and Engineering Co. [i.e., Princen and Kiss (69,95,128) and Mason et al. (66,127,137,138)]. Both groups used oil-in-water emulsions, but whereas Princen and Kiss used “typical” polydisperse emulsions with a mean radius of 5–10 μm , Mason and co-workers opted for submicron, monodisperse “Bibette emulsions.” The term “monodisperse” is relative; there remained some polydispersity in drop radius of about 10% and the emulsions were structurally disordered on a macroscopic scale. The mean drop size in Princen’s emulsions was at least an order of magnitude greater, which may account for some of the differences in the results. Princen and Kiss used their customized concentric-cylinder viscometer exclusively, either in steady shear with wall slip (to give the yield stress and viscosity) or as a constant-strain device without wall slip (to give the static shear modulus). Mason and co-workers were more eclectic in choosing their techniques (concentric-cylinder and cone-and-plate geometries in steady-shear and dynamic modes, as well as optical techniques).

Shear Modulus. Princen and Kiss (95) used a series of well-characterized, polydisperse oil-in-water emulsions of essentially identical Sauter mean drop size, R_{32} , and drop size distribution but varying dispersed-phase volume fraction, ϕ . Their modified Couette viscometer was purposely equipped with ground and grooved glass cylinders to eliminate wall slip,* and the emulsion was strained by turning the outer cylinder over a small, precisely measured angle in the linear elastic regime. From the measured stress at the inner cylinder, the static shear modulus, G , can be obtained in a straightforward manner. The results in Fig. 30 show that over the range considered ($0.75 < \phi < 0.98$), $GR_{32}/\sigma\phi^{1/3}$ varies linearly with ϕ , and we can write

$$G = 1.77 \frac{\sigma}{R_{32}} \phi^{1/3} (\phi - 0.712) = 1.77 \frac{\sigma}{R_{32}} \phi^{1/3} (\phi - \phi_0) \quad (85)$$

where $\phi_0 = 0.712$ can be identified as the “rigidity-loss transition” for the particular size distribution in these emulsions. This is surprisingly close to that for ideal close packing of monodisperse spheres ($\phi_0 = 0.7405$) but clearly in excess of that for random close packing of monodisperse spheres ($\phi_0 \approx 0.64$). The exact value of ϕ_0 is expected to depend somewhat on the details of the drop size distribution.

*This fact was unfortunately misrepresented in Ref. 66.

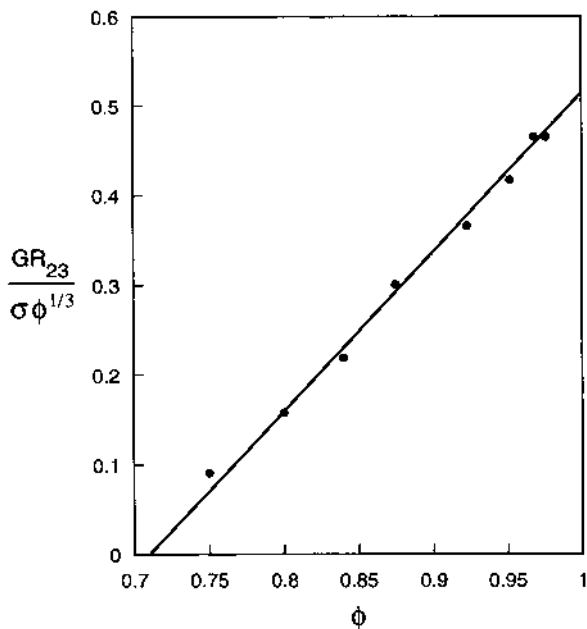


Figure 30 Scaled static shear modulus, $GR_{32}/\sigma\phi^{1/3}$, versus ϕ for typical polydisperse emulsions. Solid points are experimental data; the solid line is drawn according to Eq. (85). (From Ref. 95, with permission from Academic Press.)

In the “dry-foam” limit ($\phi = 1$), Eq. (85) reduces to

$$G_{\phi=1} = 0.509 \frac{\sigma}{R_{32}} \quad (86)$$

As indicated earlier, this is in close agreement with various theoretical estimates.

It may be argued which mean drop size is most appropriate for describing the rheology of polydisperse systems. The selection of R_{32} is based on limited evidence (69) and some other mean might ultimately turn out to be preferable. (See, however, the postscript in Sect. IX.)

A simple extension of the perfectly ordered 2D model to a 3D model would have suggested that $G = 0$ for $\phi < \phi_0 = 0.74$, with a sudden jump to an almost constant, finite value of $G \propto \sigma\phi^{1/3}/R$ for $\phi > 0.74$ [cf. Eq. (72)]. As discussed earlier, it is now generally agreed that the absence of the discontinuity and the essentially linear dependence on ϕ above ϕ_0 , found experimentally, is due to structural disorder.

Mason et al. (66) used small-amplitude, dynamic, oscillatory methods (both in cone-and-plate and concentric-cylinder geometries) to probe the viscoelastic properties [i.e., the storage (elastic) and loss (viscous) moduli, G' and G'' , respectively] as a function of frequency, ω . No mention is made of wall-induced instability or end and edge effects. Having roughened the viscometer walls, the authors claim that wall slip was nonexistent. At low frequencies, G' reached a plateau that may be equated with the static shear modulus, G . Plots of the scaled modulus, GR/σ , versus the effective volume fraction, ϕ_e , for four emulsions of different drop size essentially overlapped, as expected. The drops were so small that significant corrections had to be made to the nominal volume fractions to account for the finite (estimated) film thickness, h , according to Eq. (1). In the dry-foam limit ($\phi_e = 1$), the scaled modulus approached a value of about 0.6, which is reasonably close to Princen's value of 0.51, but even for $\phi < 1$, the data of the two groups are remarkably similar. For example, for $\phi_e = 0.85$ and 0.75, Mason et al. show values for GR/σ of about 0.30 and 0.10, respectively, whereas Eq. (85) yields 0.23 and 0.061, respectively, for GR_{32}/σ . The differences are roughly commensurate with the scatter in Mason's data. At any rate, the difference in polydispersity in the two sets of emulsions, or some experimental factor in either study (end/edge effects?), may well explain these minor systematic discrepancies.

Overall, Mason et al. found that their data can be described by

$$G \approx 1.7 \frac{\sigma}{R} \phi (\phi - 0.64) = 1.7 \frac{\sigma}{R} \phi (\phi - \phi_0) \quad (87)$$

where $\phi_0 \approx 0.64$ is the value for random close packing of monodisperse spheres. Except for the difference in ϕ_0 , this is very similar to Eq. (85).

Because of the limited sensitivity of their viscometer and the increased potential effect of a gradient in ϕ due to gravity, Princen et al. did not explore the range of $\phi < 0.75$ and reasonably assumed that the linear behavior in Fig. 30 continues down to $G = 0$ at $\phi = \phi_0 \approx 0.71$. It is unclear what significance, if any, must be attached to the apparent difference in ϕ_0 found in the two studies. Had it been possible to properly explore that regime, Princen's data might have shown some curvature for $\phi < 0.75$ and a similar smooth decline in G toward zero at $\phi_0 \approx 0.64$. More likely, the difference is real and simply attributable to the differences in polydispersity and associated random packing density. Another factor of potential significance is the large difference in mean drop size. The drops in Mason's emulsions were submicron and, therefore, Brownian, which may contribute an entropic (thermal) component to the modulus, as well as affect the packing density.

Direct support for Eq. (85) has been reported by, among others, Taylor (139), Jager-Lézer et al. (140), Pal (141), and Coughlin et al. (142). Indirect support has been obtained by Langenfeld et al. (143), who compared the specific surface areas of a number of water-in-oil emulsions as determined by two independent methods: (a) from the measured shear modulus—which yields R_{32} from Eq. (85), and thus the specific surface area from $3\phi/R_{32}$ —and (b) from small-angle neutron scattering. The agreement was very satisfactory.

Yield Stress and Shear Viscosity. Using their modified concentric-cylinder viscometer—equipped in this case with polished glass inner and outer cylinders to allow unimpeded wall slip and a mercury pool to eliminate the lower end effect—Princen and Kiss (128) determined the yield stresses, τ_0 , and effective viscosities, $\mu_e(\dot{\gamma})$, of a series of well-characterized, polydisperse oil-in-water emulsions. They empirically established that in all cases, the all-slip/no-flow regime at slow steady shear was characterized by a linear dependence of τ_1 on ω/τ_1 (where τ_1 is the stress on the inner cylinder and ω is the angular velocity of the outer cylinder). The stress at which the data deviated from this linearity was identified as the yield stress. At higher angular velocity, it was reasonably assumed that the same linear slip behavior continued to operate, which permitted a straightforward slip correction. Using conventional rheometric analyses, the stress and viscosity were finally obtained as a function of shear rate.

The yield stress data could be expressed in the form

$$\tau_0 = \frac{\sigma}{R_{32}} \phi^{1/3} Y(\phi) \quad (88)$$

The experimental values of $Y(\phi)$ are shown in Fig. 31 and can be empirically fit to

$$Y(\phi) = -0.080 - 0.114 \log(1 - \phi) \quad (89)$$

Equation (89) should be used only within the range considered (i.e., $0.83 < \phi < 0.98$).

Data by Pal (141) support Eqs. (88) and (89), once the volume fraction is corrected for a finite film thickness of 90 nm. Earlier data by Princen (69) are consistently somewhat higher, probably because of significant end effects in the original, unmodified viscometer.

Figures 32 and 33 show the fully corrected plots of shear stress versus shear rate. Taking account of small differences in the measured interfacial tensions, all data could be accurately represented by

$$\tau = \tau_0 + 32.0(\phi - 0.73) \frac{\sigma}{R_{32}} \text{Ca}^{1/2} = \tau_0 + 32.0(\phi - 0.73) \left(\frac{\sigma \mu \dot{\gamma}}{R_{32}} \right)^{1/2} \quad (90)$$

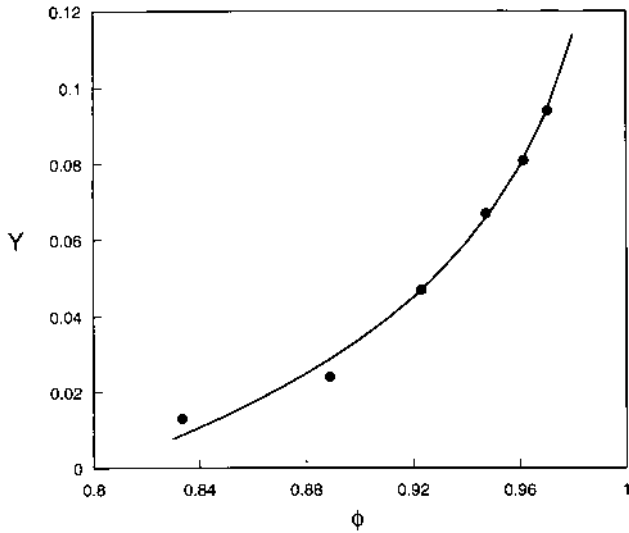


Figure 31 Yield stress function $Y(\phi) = \tau_0 R_{32} / \sigma \phi^{1/3}$ versus ϕ for typical polydisperse emulsions. Solid points are experimental data; the curve is drawn according to Eq. (89). (From Ref. 128, with permission from Academic Press.)

where μ is the viscosity of the continuous phase and Ca is the capillary number

$$Ca \equiv \frac{\mu R_{32} \dot{\gamma}}{\sigma} \quad (91)$$

which did not exceed a value of 10^{-4} in any of the experiments.

For the effective viscosity, this leads to

$$\mu_e \equiv \frac{\tau}{\dot{\gamma}} = \frac{\tau_0}{\dot{\gamma}} + 32.0(\phi - 0.73)\mu Ca^{-1/2} = \frac{\tau_0}{\dot{\gamma}} + 32.0(\phi - 0.73) \left(\frac{\sigma \mu}{R_{32} \dot{\gamma}} \right)^{1/2} \quad (92)$$

where τ_0 is given by Eqs. (88) and (89). Again, Eq. (92) should not be used outside the range considered. It is interesting to point out that, as with so many other properties, the viscous term tends to zero at $\phi = \phi_0 \approx 0.73$.

It is encouraging that Eqs. (90) and (92) have the same form as Eqs. (84) and (83), respectively, except for the exponent of the capillary number. Several reasons for this difference have been advanced (128), including the neglect of T1 rearrangements and disjoining pressure effects

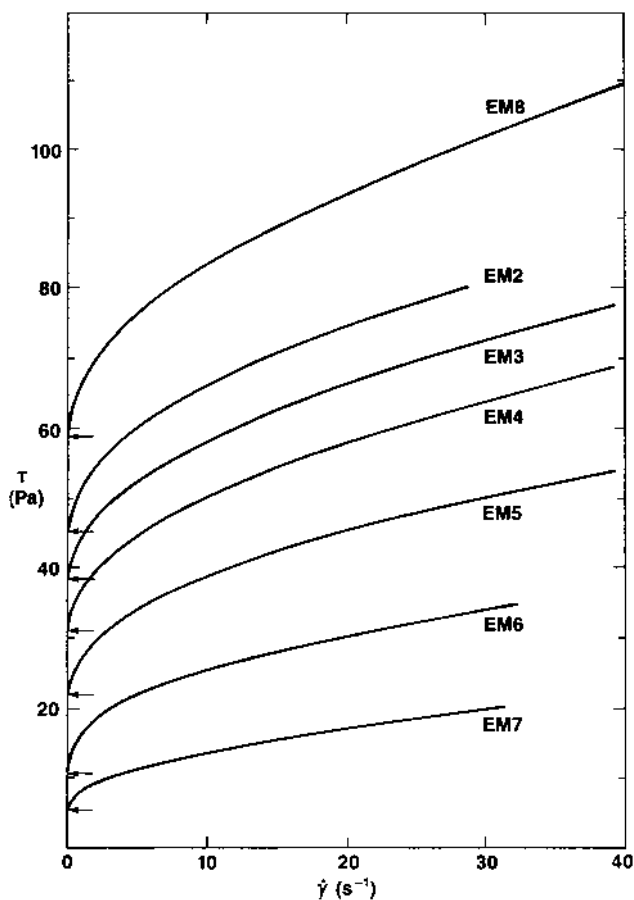


Figure 32 Fully corrected plots of shear stress vs shear rate for series of typical polydisperse emulsions. Arrows indicate the yield stress, τ_0 . Emulsions EM2–7 have the same drop size ($R_{32} = 10.1 \pm 0.1 \mu\text{m}$) but different volume fractions ($\phi = 0.9706, 0.9615, 0.9474, 0.9231, 0.8889, \text{ and } 0.8333$, respectively). For EM8, $R_{32} = 5.73 \mu\text{m}$ and $\phi = 0.9474$. (From Ref. 128, with permission from Academic Press.)

in the original model. At any rate, considering that this is the first and only systematic study of its kind, it is not yet clear how generally applicable Eqs. (90) and (92) will turn out to be. Although some other qualitative experimental support exists (144–146), there is a great need for additional, careful studies to explore this area further. It may be significant in this context that Liu et al. (147), using diffusing-wave spectroscopy [a novel light-scattering

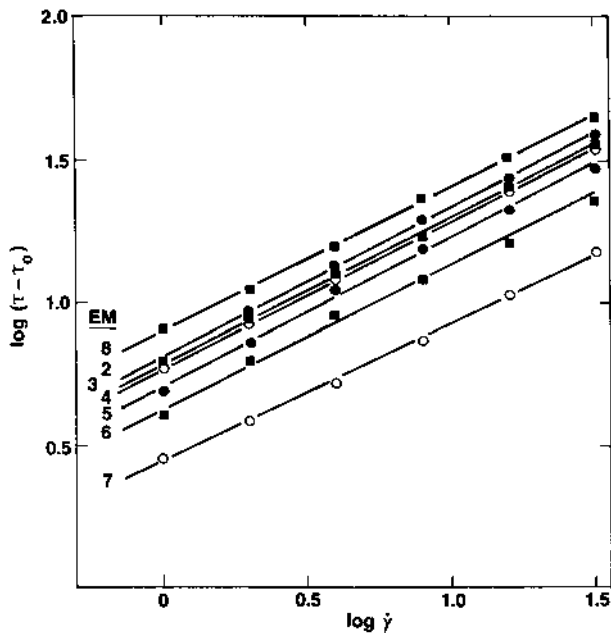


Figure 33 Plots of $\log(\tau - \tau_0)$ versus shear rate for same emulsions as in Fig. 32. In all cases, the slope is very close to $1/2$. (From Ref. 128, with permission from Academic Press.)

technique (148)] have found a contribution to the dynamic shear modulus that is proportional to $\omega^{1/2}$ (or $Ca^{1/2}$) and increases roughly linearly with volume fraction. Mason et al. (138) investigated the steady-shear behavior of some monodisperse emulsions in the low- ϕ range. They found that the viscous stress contribution varies as $\dot{\gamma}^{2/3}$ for $\phi=0.58$ and as $\dot{\gamma}^{1/2}$ for $\phi=0.63$. For $\phi > 0.65$, no clear power-law behavior was observed. These authors claim that meaningful steady-shear measurements cannot be made on emulsions of higher volume fractions because of the occurrence of “inhomogeneous” strain rates. They presumably refer to the fact that, for example, in a concentric-cylinder viscometer, only part of the emulsion (i.e., within a given radius) is being sheared, whereas the outer part is not. However, this situation, common to all yield-stress fluids, has been well recognized and analyzed in the rheology literature and can be handled in a quite straightforward manner (128).

Mason et al. (138) determined the yield stresses and yield strains of a series of monodisperse emulsions, using either a cone-and-plate or double-wall Couette geometry in oscillatory mode. Wall-induced coalescence and

wall slip were claimed to be absent, but no mention is made of attempts to reduce end or edge effects. Estimated film thicknesses were used to arrive at the effective volume fractions. Their data for the yield stress could be fit to

$$\tau_0 = 0.51 \frac{\sigma}{R} (\phi - 0.62)^2 \quad (93)$$

and, for high ϕ , are claimed to be “about an order of magnitude greater than those measured for polydisperse emulsions,” as given by Eqs. (88) and (89). This appears to be a misrepresentation. It is readily demonstrated that the two sets of data are, in fact, quite comparable. For example, for $\phi = 0.85$ and $\phi = 0.95$, the values of the scaled yield stress, $\tau_0 R / \sigma$, are 0.027 and 0.055 according to Eq. (93), and 0.013 and 0.067 according to Eq. (88). In fact, as $\phi \rightarrow 1$, Mason et al. predicted that the scaled yield stress reaches a limiting value of 0.074, whereas extrapolation of Princen and Kiss’s data in Fig. 31 suggest a value that is well in excess of 0.1 and perhaps as high as 0.15 [the yield stress must remain finite in this limit and use of Eq. (89) is unwarranted in this regime]. Mason et al. further assert that, at high ϕ , the yield *strain* of their monodisperse emulsions is also over an order of magnitude greater than that of the polydisperse emulsions of Princen and Kiss. This conclusion appears to be equally unfounded. In fact, the rheological behavior of concentrated emulsions appears to be remarkably unaffected by polydispersity.

We are not aware of any other systematic experimental studies that meet the criteria set out above and there remains a great need for additional careful work in this fascinating area.

VIII. ADDITIONAL AREAS OF INTEREST

Although this review covers many aspects of highly concentrated emulsions and foams, it does not deal with a number of issues that are of considerable interest. Foremost is the issue of emulsion and foam stability. A great deal of information can be gleaned from recent books on foams and conventional emulsions (17–22). Stability of highly concentrated emulsions is a rather more delicate and specialized problem. The reader may consult a number of recent publications that specifically deal with this subject (149–154).

One of the main driving forces for the recent upsurge in interest in foams—and one that has been responsible for the entrance of so many physicists into the field—has been their presumed usefulness in modeling grain growth in metals. The coarsening of foam through gas diffusion (a special form of Ostwald ripening) is thought to follow similar laws.

This, among other things, inspired the first computer simulations of foams by Weaire and co-workers and remains an active area of research (33).

As indicated, highly concentrated emulsions provide attractive starting materials for the synthesis of novel materials (e.g., polymers and membranes). Ruckenstein has been particularly active in this area. In addition to the references cited earlier (6,12–16), the reader may wish to consult a recent comprehensive review of this area (155).

IX. POSTSCRIPT

Except for some minor editing, this review is identical to [Chapter 11 in Ref. 156](#). Since then, further progress has been made. Two noteworthy examples are the following.

In a recent tour de force, Kraynik, Reinelt, and van Swol (personal communication, 2002) have carried out numerous computer simulations on the shear modulus of truly disordered, 3D, dry-foam systems, in which the degree of polydispersity was varied by over two orders of magnitude. Their work comes to two important conclusions: (a) The surface volume or Sauter mean radius R_{32} leads to a true numerical constant in Princen's Eq. (86). The choice of other means, such as the simple average radius, appears to lead to a numerical factor that varies significantly with the degree of polydispersity. Moreover, Kraynik et al. have developed strong theoretical grounds for this conclusion. Although Princen's initial choice of this particular mean was based mostly on intuition, and on very limited experimental evidence, that choice now appears to have been justified. (b) With R_{32} as the mean, Kraynik et al. found that the appropriate value of the numerical factor in Eq. (86) is 0.511, in remarkable agreement with Princen's experimental value of 0.509! Because the error in both values is estimated to be a few percent, it can be stated with considerable confidence that the constant equals 0.51 ± 0.01 . Unfortunately, the case of "wet" foams ($\phi < 1$) appears to be computationally too intensive to be similarly simulated in the foreseeable future.

In a recent *experimental* study, Ponton et al. (157) measured the shear moduli of a series of laboratory-prepared, polydisperse water-in-oil emulsions of varying volume fraction. R_{32} was used as the characteristic mean radius. The results were in very close agreement with Eq. (85) in that the value of ϕ_0 was found to be 0.714, instead of Princen's reported value of 0.712. Again, we see remarkable agreement! Unfortunately, the authors failed to measure the interfacial tension in these emulsions, so that the value of the numerical factor in Eq. (85) could not be ascertained.

ACKNOWLEDGMENTS

Special thanks are due to A. M. Kraynik for the many stimulating discussions we have had over the years, for keeping me informed on recent developments, and for kindly providing some of the unpublished results and illustrations. I have also benefited from illuminating discussions with P.-G. de Gennes and D. Weaire. My interest in these fascinating systems goes back to my years at Unilever Research, where E. D. Goddard and M. P. Aronson provided invaluable and much appreciated support and collaboration.

LIST OF SYMBOLS

Latin Symbols

a	Side of hexagon circumscribing compressed 2D drops in perfect order
a_o	Side of hexagon circumscribing uncompressed (circular) 2D drops in perfect order
a_c	Capillary length = $[\sigma/(\Delta\rho g)]^{1/2}$
c_i	Mean curvature of surface between Plateau border and drop i
C_{ij}	Mean curvature of film between drops i and j
C_t	Mean curvature of free surface of continuous phase at dispersion-atmosphere boundary
Ca	Macroscopic capillary number = $\mu a\dot{\gamma}/\sigma$ or $\mu R_{32}\dot{\gamma}/\sigma$
Ca*	Film-level capillary number = $\mu U/\sigma$
e	Number of edges of a polyhedral drop
f	Number of faces of a polyhedral drop
$f(\phi)$	Fraction of surface of confining wall “in contact” with dispersed drops
F	Stress per unit cell
F_{\max}	Maximum or yield stress per unit cell
g	Acceleration due to gravity
G	Static shear modulus
G'	Storage modulus
G''	Loss modulus
h	Film thickness
h_{eq}	Equilibrium film thickness
h_{∞}	Half the film thickness pulled out of Plateau border
H	Sample height
H_{cr}	Critical sample height for separation of continuous phase
K	Compression modulus
p_b	Pressure in Plateau border

p_c	Capillary pressure
p_i	Pressure in drop i
p_v^c	Vapor pressure of continuous phase in dispersion
$(p_v^c)_0$	Vapor pressure of bulk continuous phase
p_v^d	Vapor pressure of dispersed phase in dispersion
$(p_v^d)_0$	Vapor pressure of bulk dispersed phase
P	External pressure
r	Radius of Plateau border surfaces in 2D close-packed drops
R	Radius of spherical or circular drop
R_{av}	Average drop radius
R_{32}	Surface volume or Sauter mean drop radius
\mathfrak{R}	Gas constant
S	Surface area of compressed drops
S_0	Surface area of uncompressed (spherical or circular) drops
S_f	Surface area contained in films
T	Absolute temperature
U	Film velocity
v	Number of vertices of a polyhedral drop
V	Dispersion volume
V_1	Volume of the dispersed phase
V_2	Volume of the continuous phase in the dispersion
\bar{V}_1, \bar{V}_2	Partial molar volume of phase 1 and 2, respectively
$Y(\phi)$	Yield-stress function
z	Vertical height in dispersion column

Greek Symbols

γ	Strain
$\dot{\gamma}$	Rate of strain
$\Delta\rho$	Density difference
θ	Contact angle at film–Plateau border junction
μ	Viscosity of continuous phase
μ_d	Viscosity of dispersed phase
μ_e	Effective viscosity of dispersion
Π	Osmotic pressure
Π_d	Disjoining pressure
ρ	Density
σ	Surface or interfacial tension
τ	Stress
τ_0	Yield stress
τ_s	Stress due to dissipative processes
ϕ	Volume fraction of dispersed phase in emulsion or foam

ϕ_0	Volume fraction of close-packed spherical drops
ϕ_e	Effective volume fraction, after correction for finite film thickness
ψ	Angle between films and shear direction
ω	Frequency or angular velocity

REFERENCES

1. F. J. Almgren and J. E. Taylor, *Sci. Am.* 235, 82 (1976).
2. C. S. Smith, *Metall. Rev.* 9, 1 (1964).
3. E. B. Matzke, *Am. J. Bot.* 33, 58, 130 (1946).
4. K. J. Lissant, *J. Colloid Interf. Sci.* 22, 462 (1966).
5. K. J. Lissant, *J. Soc. Cosmet. Chem.* 21, 141 (1970).
6. K. J. Lissant and K. G. Mayhan, *J. Colloid Interf. Sci.* 42, 201 (1973).
7. A. Beerbower, J. Nixon, and T. J. Wallace, *J. Aircraft* 5, 367 (1968).
8. A. Beerbower, J. Nixon, W. Philippoff, and T. J. Wallace, *SAE Trans. Sec. 2* 76, 1446 (1968).
9. J. Nixon, A. Beerbower, and T. J. Wallace, *Mech. Eng.* 90, 26 (1968).
10. J. Nixon, and A. Beerbower, *Preprints, Div. Petrol. Chem. Am. Chem. Soc.* 14, 49 (1969).
11. K. J. Lissant, U.S. patent No. 3,892,881.
12. K. J. Lissant, B. W. Peace, S. H. Wu, and K. G. Mayhan, *J. Colloid Interf. Sci.* 47, 416 (1974).
13. J. M. Williams, *Langmuir* 4, 44 (1988).
14. E. Ruckenstein and K. Kim, *J. Appl. Polym. Sci.* 36, 907 (1988).
15. E. Ruckenstein, *Colloid Polym. Sci.* 267, 792 (1989).
16. E. Ruckenstein and J. S. Park, *Chem. Mater.* 1, 343 (1989).
17. J. Sjöblom (ed.), *Emulsions and Emulsion Stability*, Surfactant Science Series Vol. 61, Marcel Dekker, New York; 1996.
18. R. K. Prud'homme and S. A. Khan (eds.), *Foams: Theory, Measurements, and Applications*, Surfactant Science Series Vol. 57, Marcel Dekker, New York, 1996.
19. L. L. Schramm (ed.), *Foams: Fundamentals and Applications in the Petroleum Industry*, Advances in Chemistry Series No. 242, American Chemical Society, Washington, DC, 1994.
20. D. Exerowa and P. M. Kruglyakov (eds.), *Foam and Foam Films: Theory, Experiment, Application*. Studies in Interface Science Vol. 5, Elsevier, Amsterdam, 1998.
21. D. Weaire and S. Hutzler, *The Physics of Foams*, Clarendon Press, Oxford, 1999.
22. J. F. Sadoc and N. Rivier (eds.) *Foams and Emulsions*, Kluwer Academic, Dordrecht, 1999.
23. H. M. Princen, M. P. Aronson, and J. C. Moser, *J. Colloid Interf. Sci.* 75, 246, (1980).
24. H. M. Princen and A. D. Kiss, *Langmuir* 3, 36 (1987).

25. D. M. A. Buzza and M. E. Cates, *Langmuir* 9, 2264 (1993).
26. M. P. Aronson and H. M. Princen, *Nature* 286, 370 (1980).
27. M. P. Aronson and H. M. Princen, *Colloids Surfaces* 4, 173 (1982).
28. H. M. Princen, *Colloids Surfaces* 9, 47 (1984).
29. H. M. Princen, *Langmuir* 4, 164 (1988).
30. A. V. Neimark and M. Vignes-Adler, *Phys. Rev. E* 51, 788 (1995).
31. F. Bolton and D. Weaire, *Phil. Mag.* B 63, 795 (1991).
32. V. V. Krotov and A. I. Rusanov, *Mendeleev Commun.* 177 (1998).
33. J. A. Glazier and D. Weaire, *J. Phys.: Condens. Matter* 4, 1867 (1992).
34. J. A. Glazier and J. Stavans, *Phys. Rev. A* 40, 7398 (1989).
35. J. A. Glazier, S. P. Gross, and J. Stavans, *Phys. Rev. A* 36, 306 (1987).
36. J. Stavans and J. A. Glazier, *Phys. Rev. Lett.* 62, 1318 (1989).
37. J. Stavans, *Phys. Rev. A* 42, 5049 (1990).
38. J. Lucassen, S. Akamatsu, and F. Rondelez, *J. Colloid Interf. Sci.* 144, 434 (1991).
39. H. M. Princen, *J. Colloid Interf. Sci.* 71, 55 (1979).
40. H. M. Princen, *Langmuir* 2, 519 (1986).
41. P. M. Kruglyakov, D. R. Exerowa, and K. I. Khrystov, *Langmuir* 7; 1846 (1991).
42. K. Khrystov, P. Kruglyakov, and D. Exerowa, *Colloid Polym. Sci.* 257, 506 (1979).
43. K. Khrystov, D. Exerowa, and P. M. Kruglyakov, *Colloid J. (Engl. Transl.)* 50, 765 (1988).
44. D. Weaire and J. P. Kermode, *Phil. Mag. B* 50, 379 (1984).
45. S. A. Khan and R. C. Armstrong, *J. Non-Newtonian Fluid Mech.* 25, 61 (1987).
46. A. M. Kraynik, D. A. Reinelt, and H. M. Princen, *J. Rheol.* 35, 1235 (1991).
47. F. Bolton and D. Weaire, *Phil. Mag. B* 65, 473 (1992).
48. S. Hutzler and D. Weaire, *J. Phys: Condens. Matter.* 7, L657 (1995).
49. K. A. Brakke, *Exp. Math.* 1, 141 (1992).
50. A. M. Kraynik and D. A. Reinelt (private communication; to be published).
51. M.-D. Lacasse, G. S. Grest, and D. Levine, *Phys. Rev. E* 54, 5436 (1996).
52. W. Thomson (Lord Kelvin), *Phil. Mag.* 24, 503 (1887).
53. W. Thomson (Lord Kelvin), *Acta Math.* 11, 121 (1887–1888).
54. W. Thomson (Lord Kelvin), *Mathematical and Physical Papers*, Cambridge University Press, London, 1911, Vol. V, p 297.
55. H. M. Princen and P. Levinson. *J. Colloid Interf. Sci.* 120, 172 (1987).
56. D. A. Reinelt and A. M. Kraynik, *J. Colloid Interf. Sci.* 159, 460 (1993).
57. D. Weaire and R. Phelan, *Phil. Mag. Lett.* 69, 107 (1994).
58. S. Ross and H. F. Prest, *Colloids Surfaces* 21, 179 (1986).
59. D. S. Bohlen, H. T. Davis and L. E. Scriven, *Langmuir* 8, 892 (1992).
60. H. W. Schwartz, *Rec. Trav. Chim.* 84, 771 (1964).
61. H. Aref, and T. Herdtle, in *Topological Fluid Mechanics*, (H. Moffat and A. Tsinober, eds.), Cambridge University Press, New York, 1990, p. 745.
62. T. Herdtle, Ph.D. thesis, University of California, San Diego, 1991.
63. C. Monnereau and M. Vignes-Adler, *Phys. Rev. Lett.* 80, 5228 (1998).

64. S. D. Pacetti, Masters thesis, University of Houston, 1985.
65. J. Bibette, *J. Colloid Interf. Sci.* 147, 474 (1991).
66. T. G. Mason, M.-D. Lacasse, G. S. Grest, D. Levine, J. Bibette, and D. A. Weitz, *Phys. Rev. E* 56, 3150 (1997).
67. H. M. Princen, *J. Colloid Interf. Sci.* 134, 188 (1990).
68. A. M. Kraynik, M. K. Neilsen, D. A. Reinelt, and W. E. Warren, in *Foams and Emulsions*. (J. F. Sadoc and N. Rivier, eds.), Kluwer Academic, Dordrecht, 1999, pp. 259–286.
69. H. M. Princen, *J. Colloid Interf. Sci.* 105, 150 (1985).
70. B. V. Derjaguin, *Kolloid Z.* 64, 1 (1933).
71. S. Ross, *Ind. Eng. Chem.* 61, 48 (1969).
72. I. D. Morrison and S. Ross, *J. Colloid Interf. Sci.* 95, 97 (1983).
73. H. B. Hollinger, *J. Colloid Interf. Sci.* 143, 278 (1991).
74. T. L. Crowley, *Langmuir* 7, 430 (1991).
75. T. L. Crowley and D. G. Hall, *Langmuir* 9, 101 (1993).
76. M. Blackman, *Trans. Faraday Soc.* 44, 205 (1948).
77. J. O. Sibree, *Trans. Faraday Soc.* 30, 325 (1934).
78. A. David and S. S. Marsden, in *44th Annual Meeting, Society of Petroleum Engineers*, 1969, paper 2544.
79. V. Sanghani and C. U. Ikoku, *Trans. ASME* 105, 362 (1983).
80. B. J. Mitchell, *Oil Gas J.* 96 (1971).
81. S. H. Raza and S. S. Marsden, *Soc. Petrol. Eng. J.* 7, 359 (1967).
82. R. J. Mannheimer, *J. Colloid Interf. Sci.* 40, 370 (1972).
83. J. P. Heller and M. S. Kuntamukkula, *Ind. Eng. Chem.* 26, 318 (1987).
84. J. H. Aubert, A. M. Kraynik and P. B. Rand, *Sci. Am.* 254, 58 (1986).
85. A. M. Kraynik, *Annu. Rev. Fluid Mech.* 20, 325 (1988).
86. D. Weaire and M. A. Fortes, *Adv. Phys.* 43, 685 (1994).
87. H. M. Princen, *J. Colloid Interf. Sci.* 91, 160 (1983).
88. R. K. Prud'homme, in *Annual Meeting of the Society of Rheology*, 1981.
89. S. A. Khan, Ph.D. thesis, Massachusetts Institute of Technology, 1985.
90. S. A. Khan and R. C. Armstrong, *J. Non-Newtonian Fluid Mech.* 22, 1 (1986).
91. A. M. Kraynik and M. G. Hansen, *J. Rheol.* 30, 409 (1986).
92. S. Hutzler, D. Weaire, and F. Bolton, *Phil. Mag. B* 71, 277 (1995).
93. B. Derjaguin, *Kolloid Z.* 64, 1 (1933).
94. D. Stamenović and T. A. Wilson, *J. Appl. Mech.* 51, 229 (1984).
95. H. M. Princen and A. D. Kiss, *J. Colloid Interf. Sci.* 112, 427 (1986).
96. D. Stamenović, *J. Colloid Interf. Sci.* 145, 255 (1991).
97. B. Budiansky and E. Kimmel, *J. Appl. Mech.* 58, 289 (1991).
98. D. A. Reinelt, *J. Rheol.* 37, 1117 (1993).
99. A. M. Kraynik and D. A. Reinelt, *Forma* 11, 255 (1996).
100. D. A. Reinelt and A. M. Kraynik, *J. Fluid Mech.* 311, 327 (1996).
101. A. M. Kraynik and D. A. Reinelt, *J. Colloid Interf. Sci.* 181, 511 (1996).
102. A. M. Kraynik and D. A. Reinelt, *Proceedings of the XIIIth International Congress on Rheology*, 1996, p. 625.
103. A. M. Kraynik and D. A. Reinelt, *Chem. Eng. Commun.* 148/150, 409 (1996).

104. D. M. A. Buzza and M. E. Cates, *Langmuir* 10, 4502 (1994).
105. D. C. Morse and T. A. Witten, *Europhys. Lett.* 22, 549 (1993).
106. M.-D. Lacasse, G. S. Grest, D. Levine, T. G. Mason, and D. A. Weitz, *Phys. Rev. Lett.* 76, 3448 (1996).
107. D. M. A. Buzza, C.-Y. D. Lu, and M. E. Cates, *J. Phys. II (France)* 5, 37 (1995).
108. A. M. Kraynik and M. G. Hansen, *J. Rheol.* 31, 175 (1987).
109. X. Li, H. Zhu and C. Pozrikidis, *J. Fluid. Mech.* 286, 379 (1995).
110. L. W. Schwartz and H. M. Princen, *J. Colloid Interf. Sci.* 118, 201 (1987).
111. K. J. Mysels, K. Shinoda, and S. Frankel, *Soap Films: Studies of Their Thinning and a Bibliography*, Pergamon Press, New York, 1959.
112. L. Landau and B. Levich, *Acta Physicochim. URSS* 17, 42 (1942).
113. F. P. Bretherton, *J. Fluid Mech.* 10, 166 (1961).
114. L. W. Schwartz, H. M. Princen, and A. D. Kiss, *J. Fluid Mech.* 172, 259 (1986).
115. K. J. Mysels and M. C. Cox, *J. Colloid Interf. Sci.* 17, 136 (1962).
116. J. Lyklema, P. C. Scholten, and K. J. Mysels, *J. Phys. Chem.* 69, 116 (1965).
117. G. F. Teletzke, H. T. Davis, and L. E. Scriven, *Rev. Phys. Appl.* 23, 989 (1988).
118. J. Lucassen, in *Anionic Surfactants: Physical Chemistry of Surfactant Action*. (E. H. Lucassen-Reijnders, ed), Surfactant Science Series Vol. 11, Marcel Dekker, New York, 1981, p. 217.
119. D. A. Reinelt and A. M. Kraynik, *J. Colloid Interf. Sci.* 132, 491 (1989).
120. D. A. Reinelt and A. M. Kraynik, *J. Fluid Mech.* 215, 431 (1990).
121. D. A. Edwards, H. Brenner, and D. T. Wasan, *J. Colloid Interf. Sci.* 130, 266 (1989).
122. D. A. Edwards and D. T. Wasan, *J. Colloid Interf. Sci.* 139, 479 (1990).
123. D. A. Edwards and D. T. Wasan, in *Foams: Theory, Measurements, and Applications*. (R. K. Prud'homme and S. A. Khan, eds), Surfactant Science Series Vol. 57, Marcel Dekker, New York, 1996, p189.
124. T. Okuzuno and K. Kawasaki, *J. Rheol.* 37, 571 (1993).
125. T. Okuzono and K. Kawasaki, *Phys. Rev. E* 51, 1246 (1995).
126. Y. Jiang, P. J. Swart, A. Saxena, M. Asipauskas, and J. A. Glazier, *Phys. Rev. E* 59, 5819 (1999).
127. T. G. Mason, J. Bibette, and D. A. Weitz, *Phys. Rev. Lett.* 75, 2051 (1995).
128. H. M. Princen and A. D. Kiss, *J. Colloid Interf. Sci.* 128, 176 (1989).
129. H. M. Princen, I. Y. Z. Zia, and S. G. Mason, *J. Colloid Interf. Sci.* 23, 99 (1967).
130. J. L. Cayias, R. S. Schechter, and W. H. Wade. in *Adsorption at Interfaces* (K. L. Mittal, ed), ACS Symposium Series No. 8, American Chemical Society, Washington, DC, 1975, p. 234.
131. R. W. Whorlow, *Rheological Techniques*, Ellis Horwood, Chichester, 1980.
132. H. M. Princen, *J. Rheol.* 30, 271 (1986).
133. P. V. Liddell and D. V. Boger, *J. Non-Newtonian Fluids* 63, 235 (1996).
134. A. S. Yoshimura and R. K. Prud'homme, *Soc. Petrol Eng.* 735 (1988).
135. A. S. Yoshimura and R. K. Prud'homme, *J. Rheol.* 32, 53 (1988).
136. P. Brunn, M. Müller and S. Bschorer, *Rheol. Acta* 35, 242 (1996).
137. T. G. Mason and D. A. Weitz, *Phys. Rev. Lett.* 74, 1250 (1995).

138. T. G. Mason, J. Bibette, and D. A. Weitz, *J. Colloid Interf. Sci.* 179, 439 (1996).
139. P. Taylor, *Colloid Polym. Sci.* 274, 1061 (1996).
140. N. Jager-Lézer, J.-F. Tranchant, V. Alard, C. Vu, P. C. Tchoreloff, and J.-L. Grossiord, *Rheol. Acta* 37, 129 (1998).
141. R. Pal, *Colloid Polym. Sci.* 277, 583 (1999).
142. M. F. Coughlin, E. P. Ingenito, and D Stamenović, *J. Colloid Interf. Sci.* 181, 661 (1996).
143. A. Langenfeld, F. Lequeux, M.-J. Stébé, and V. Schmitt, *Langmuir* 14, 6030 (1998).
144. F. van Dieren, in *Theoretical and Applied Rheology*. (P. Moldenaers and R. Keunings, eds.), *Proceedings of the XIth International Congress on Rheology* Elsevier, Amsterdam 1992, p. 690.
145. Y. Otsubo and R. K. Prud'homme, *Soc. Rheol. (Japan)* 20, 125 (1992).
146. Y. Otsubo and R. K. Prud'homme, *Rheol. Acta* 33, 303 (1994).
147. A. J. Liu, S. Ramaswamy, T. G. Mason, H. Gang, and D. A. Weitz, *Phys. Rev. Lett.* 76, 3017 (1996).
148. D. J. Pine, D. A. Weitz, P. M. Chaikin, and E. Herbolzheimer, *Phys. Rev. Lett.* 60, 1134 (1988).
149. E. Ruckenstein, G. Ebert, and G. Platz, *J. Colloid Interf. Sci.* 133, 432 (1989).
150. H. H. Chen and E. Ruckenstein, *J. Colloid Interf. Sci.* 138, 473 (1990).
151. H. H. Chen and E. Ruckenstein, *J. Colloid Interf. Sci.* 145, 260 (1991).
152. M. P. Aronson, K. Ananthapadmanabhan, M. F. Petko, and D. J. Palatini, *Colloids Surfaces A* 85, 199 (1994).
153. M. P. Aronson and M. F. Petko, *J. Colloid Interface Sci.* 159, 134 (1993).
154. J. Bibette, D. C. Morse, T. A. Witten and D. A. Weitz, *Phys. Rev. Lett.* 69, 2439 (1992).
155. E. Ruckenstein, *Adv. Polym. Sci.* 127, 1 (1997).
156. H. M. Princen, in *Encyclopedic Handbook of Emulsion Technology*. (J. Sjöblom, ed.), Marcel Dekker, New York, 2000, p. 243.
157. A. Ponton, P. Clément, and J. L. Grossiord, *J. Rheol.* 45, 521 (2001).